Annu. Rev. Nucl. Part. Sci. 2004. 54:315–59
doi: 10.1146/annurev.nucl.54.070103.181244

DIRECT DETECTION OF DARK MATTER

Richard J. Gaitskell
Department of Physics, Brown University, Providence, Rhode Island 02912-1843;
email: Richard_Gaitskell@Brown.edu

Key Words WIMPs, axions, cold dark matter, SUSY, dark matter halo

PACS Codes 95.35.+d, 95.30.Cq, 98.62.Gq

■ **Abstract** This article reviews the astrophysics and cosmological evidence for nonbaryonic dark matter (DM). It covers historical, current, and future experiments that look for direct evidence of particle DM. In addition, it surveys the underlying particle theories that provide some guidance about expected event rates, and the future prospects for the discovery of DM. A number of recent theoretical papers, making calculations in SUSY-based frameworks, show a spread of many (>5) orders of magnitude in the possible interaction rates for models consistent with existing cosmological and accelerator bounds. Within this decade, it seems likely that DM searches will be successful, or at the very least rule out a broad class of the currently most favored DM models.

CONTENTS

18 Aug 2004 18:39 AR AR228-NS54-10.tex AR228-NS54-10.sgm LaTeX2e(2002/01/18) P1: JRX

1. INTRODUCTION

1.1. Pursuit of the Grail

Within the field of direct detection of dark matter (DM), it is very encouraging to see so many of the technologies proposed in the past decade coming to fruition. Latest results for direct detection of weakly interacting massive particles (WIMPs) can now set limits at a 90% CL of <1 evt/kg/week (above 10 $keV_{\rm r}$ threshold in germanium). Many other experiments are also able to set limits within an order of magnitude above this value. It seems likely that in the next few years we will continue to see a range of experiments all vying to set the best sensitivity limits. In the past five years there has been an overall acceleration in the rate of progress of the field, as measured by space carved out in the log-log sensitivity plots (see Figure 7, color insert), when compared to the past two decades in which searches have been conducted (see Figure 1, color insert). Experiments continue to test models of supersymmetry (SUSY) at the upper regions predicted. The progress of accelerator bounds on SUSY from the final analyses of LEP data through 2002 had been reducing the predicted direct search rates. Now it seems likely that we will have to await the final analyses of the Tevatron, or the LHC data in 2007, for significant new accelerator constraints and potential SUSY discovery.

A common experimental challenge in direct WIMP searches has been how to run a few detector units reliably for periods of many months in order to collect statistically significant exposures. Of course, some collaborations are already taking long-term running for granted. The new challenge will be scaling target masses up significantly so that event rates toward sensitivities of 1 evt/100 kg/y can be achieved. In order to make interesting measurements of WIMP interaction populations, detectors at the 1 tonne scale will be required before the end of the decade.

In addition, continued improvement in the sensitivity of axion search experiments means they continue to test the theoretically favored parameter space.

1.2. Current Cosmology

Given current astrophysical and cosmological data, it remains clear that $>95\%$ of the composition of the universe is still unknown. The unidentified components of this dark side are "known unknowns" (1), in that their general properties are understood but the specific composition has yet to be determined. There appears to be a requirement for a dark baryonic component (a few percent, mostly known), a nonbaryonic cold dark matter (CDM) component ($\sim$25%, unknown composition), and a dark energy component ($\sim$70%, great uncertainty in generating mechanism),

18 Aug 2004 18:39 AR AR228-NS54-10.tex AR228-NS54-10.sgm LaTeX2e(2002/01/18) P1: JRX

where the percentages are as a total fraction of the composition of the universe. The luminous material in the universe is $\lesssim$1% of the total composition. This section focuses on what is currently known about the nonbaryonic DM component.

1.2.1. HOW STRONG IS THE CASE FOR COLD DARK MATTER? In the early 1930s, Zwicky measured the velocity dispersion of eight galaxies in the Coma cluster (2). The magnitudes of the velocities were too high to be consistent with gravitational confinement based on the potential well arising from the visible matter alone. His initial estimate was that the stars could be only 0.5% of the total mass that was influencing the galaxies. While modern reevaluations of both the distance scale and Hubble parameter have reduced the apparent disparity in his data, the main conclusion is still robust, and this remains startling evidence for the existence of DM.

So startling, in fact, that it wasn't until the 1970s that this problem started to be looked at seriously. Data were being accumulated on the rotational velocities of spiral galaxies, and it was clear that these data also required significant additional DM. Under simple Newtonian analysis the circular rotational velocity of an object will be given by $v(r) = \sqrt{GM(r)/r}$, where $M(r)$ is the mass enclosed by the orbit, and G is Newton's gravitational constant. Beyond the radius at which the visible matter distribution appears to end, one would expect the velocity to fall as $\propto 1/\sqrt{r}$. Instead the rotational velocity for most galaxies studied appears to rise for small radii, and then asymptote to a constant $v \simeq$ 100–300 km/s for arbitrarily large radii, constrained only by our ability to find some remaining observable material with which to measure the velocity (3–5). The most common explanation for flat rotation curves is to assume that the disk galaxies are immersed in an extended DM halo such that $M(r)/r \sim$constant at large distances. A self-gravitating ball of ideal gas at a uniform temperature would have such a profile (5).

At this stage, we need to introduce a quantitative measure for the composition of the universe. The contribution from a component with density ρ_x can be given as a fraction of the critical density

$$\rho_c = (3H_0^2/8\pi G) \approx 1.88 \times 10^{-26} h^2 \,\mathrm{kg\ m^{-3}}$$
$$\approx 10.5 h^2 \,\mathrm{keV\ c^{-2}\ cm^{-3}},$$

such that for a particular component x,

$$\Omega_x = \rho_x/\rho_c.$$

H_0 is the present value of the Hubble constant; h is the dimensionless form of H_0 in units of 100 km/s/Mpc. The current experimental value for h is $\sim$0.7 with an uncertainty of $\sim$5%.

It has been established through extensive surveys that all the luminous matter in the universe is $\Omega_{\mathrm{lum}} \lesssim 0.01$. If an analysis of the rotation curves of galaxies implies >90% of the mass in the galaxies is dark, then the implication is that $\Omega_{\mathrm{DM}} \approx 0.1$. In reality, this is a lower bound, since most rotation curves remain flat

out to the largest radii at which they can be measured, and because it is suggested that the DM halos extend out further one concludes that $\Omega_{\rm DM} \geq 0.1$. At the edge of the above constraints it is still possible that some form of baryonic DM could be responsible for the dark halos. Direct searches for massive compact halo objects (MACHOs) were conducted using microlensing. The results from these searches indicated that <25% of the dark halo could be due to these objects in the mass range $2 \times 10^{-7}\, M_{\rm sun} < M < 1\, M_{\rm sun}$ at 95% CL (under standard halo assumptions for the Milky Way of 4×10^{11} solar masses inside 50 kpc) (6, 7). Recent data from the Hubble Deep Field Space Telescope also suggest that the halo is $\leq$5% white dwarfs.

The analysis of larger objects, such as clusters and superclusters of galaxies, is more involved than that for galaxy rotation, but these data also strongly support the existence of an even larger DM component in the universe (8). These measurements include observations of velocity flows, x-ray emission temperatures in clusters, and gravitational lensing methods. What is equally significant is that as these techniques have been refined in the past 10 years the predictions for the total matter component have converged to a very similar range of $\Omega_{\rm m} \approx 0.2$–$0.3$.

As a separate exercise, Peebles (9) proposed the idea that some form of cold dark matter (CDM) was required to reconcile the observed power spectrum of structure formation in the universe with the stringent observational upper limits that were being placed on the relative homogeneity of the cosmic microwave background (CMB). The CMB represents a snapshot of the baryonic matter distribution ~300,000 years after the Big Bang. This idea was distinct from the DM required to reconcile the deviation from Newtonian predictions of luminous matter in galaxies/galaxy clusters. The model requires that in the early universe CDM clumped first through gravitational attraction and that this structure was followed by baryonic matter when neutral atoms (post-CMB, surface of last scattering for photons) formed (10). The magnitude of the fluctuations in the CMB was finally established by the COBE satellite (11), and they have been measured to greater degrees of precision by later experiments, including the very recent results from the Wilkinson Microwave Anisotropy Probe (WMAP) satellite (12–16).

Some have argued that DM is not necessary to explain the rotation curves of galaxies, and suggested a modified Newtonian dynamics in its place. Recent Sloan Digital Sky Survey (SDSS) data are providing a useful test of the precise halo density distribution at larger radii, which is consistent with the $1/r^3$ predicted by CDM, and in contradiction with many of the predictions of modified Newtonian dynamics (17).

Models of Big Bang nucleosynthesis (BBN) (18, 19) provide a very direct constraint on the amount of baryonic matter in the universe based on the observed primordial abundances of light elements. The latter data are most heavily influenced by D/H abundance measurements in Lyman-α absorption spectra (20). A value for $\Omega_{\rm b}h^2 = 0.022 \pm 0.02$, $\Omega_{\rm b} \approx 4.5\%$ (where b stands for baryons) is clearly too low to permit baryons to form the majority of the matter in the universe.

Combining the latest CMB data from WMAP (16) with galaxy redshift surveys from SDSS, 2dF Galaxay Redshift Survey, and the data from type I supernovae (SNIa) observations (21–23) allows the precision determination of many cosmological parameters (24). An example of a combined analysis from Tegmark et al. (25) is shown in Figure 2 (see color insert). The CMB measurement provides a direct measurement of the spatial flatness of the universe,

$$\Omega_{\mathrm{TOTAL}} = \Omega_{\mathrm{m}} + \Omega_{\Lambda} = 1.02 \pm 0.02,$$

where $\Omega_{\mathrm{TOTAL}} = 1$ is expected for a flat universe, and Ω_{Λ} is the contribution from the dark energy component.

It should be noted that the individual measurement techniques often show clear degeneracies in their ability to predict individual parameters, fixing instead combinations of the traditionally sought-after values. However, the combination of the data allows a surprising level of precision in the parameters. In addition, where genuinely independent predictions are possible for parameters, remarkable concordance is obtained. Assuming $h = 0.7$, one finds (with 1σ errors) that

$$\Omega_{\mathrm{b}} = 4.6 \pm 0.1\%$$

$$\Omega_{\mathrm{nbm}} = 22 \pm 2\%$$

$$\Omega_{\Lambda} = 73 \pm 4\%,$$

although it should be pointed out that a greater range of allowed values are permitted when model assumptions are varied. Ω_{b}, the baryonic component, is in very good agreement with BBN predictions. Ω_{nbm} is the nonbaryonic component of DM. At the present time there appears to have developed a "standard cosmological model" (also known as Λ-CDM), albeit one that leaves us somewhat in the dark about the whys and the wherefores.

1.2.2. NONBARYONIC DARK MATTER A convincing case seems to exist for nonbaryonic DM. Elementary particles, often arising from as-yet-undiscovered but well-motivated physics, dominate the field. The DM density in the neighborhood of our solar system is expected to be $\rho_{\mathrm{DM}} \sim 0.3\,\mathrm{GeV\,cm^{-3}}$, although, as discussed below, this varies by $\sim 2^{\pm 1}$ in some halo models. We now discuss some of the candidate particles, many of which are illustrated in Figure 3.

Standard-model neutrinos are now known to be massive. A lower limit on this mass stems from the observation of neutrino oscillations in atmospheric neutrino data (26),

$$\nu_{\mu} \rightarrow \nu_{\tau} \quad \Delta m^2_{23} \sim 3 \times 10^{-3}\,\mathrm{eV^{-2}},$$

which, when combined with solar neutrino oscillation data (27), implies that the most massive neutrino must have a mass $\gtrsim 0.05$ eV. The contribution of neutrinos

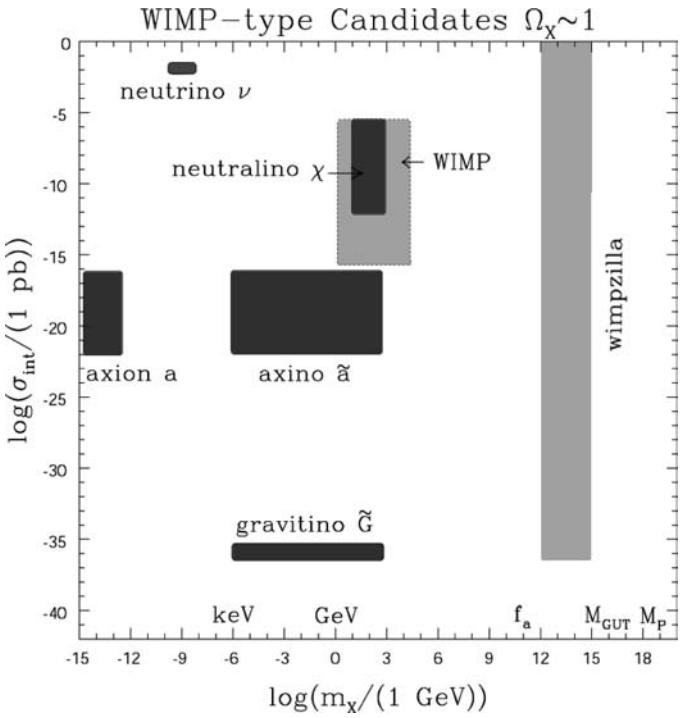

Figure 3 A schematic representation of some well-motivated WIMP-type particles. σ_{int} represents a typical order-of-magnitude estimate of the interaction strength with ordinary matter. m_χ is the mass of the candidate. The neutrino provides hot dark matter, which is disfavored. The region marked "WIMP" includes several possible candidates, e.g., from Kaluza-Klein scenarios. Reproduced from Reference (58).

to the universe follows the relation

$$\Omega_\nu h^2 = \sum_{i=1}^{3} \frac{g_i m_i}{90\,\text{eV}},$$

where $g_i = 1$ for Majorana neutrinos (own antiparticle), and $g_i = 2$ for Dirac neutrinos (distinct antiparticle), which suggests a minimum contribution to the universe composition (for a Majorana neutrino) of $\Omega_\nu h^2 \gtrsim 0.0006$. So standard-model neutrinos are DM. However, they are hot. An excess amount of relativistic particles during the epoch of galaxy formation would wash out small-scale structure, preventing agreement with the matter density distribution observed today. A combination of galaxy clustering measurements, CMB, and observations of Lyman-α forest gives an upper limit on light neutrino contribution of (24)

$$\Omega_\nu h^2 < 0.0076.$$

This limit applies to all forms of hot DM, and so we mainly concern ourselves here with cold DM candidates, since they must form the dominant matter component.

Clearly, candidates for CDM must satisfy several conditions. They must (*a*) interact very weakly, or not at all, with electromagnetic radiation ("dark" matter); (*b*) have a cosmologically interesting (preferably dominant) relic density; and (*c*) be stable on time scales comparable with the age of the universe (otherwise they would have decayed).

A strongly favored candidate for CDM is the WIMP, with a mass $\sim$10 GeV–few TeV, with interaction cross sections of the order of the weak scale. Their relic density can be calculated reliably if the WIMPs were in thermal equilibrium with the other standard-model particles in the early stages ($<$1 ns) following the Big Bang. As the temperature, T, of the universe cools, the density of the more massive particles with masses $m_\chi > T$ will become exponentially (Boltzmann) suppressed. When the expansion rate of the universe, H, exceeds the particle annihilation/creation rate, the WIMPs drop out of thermal equilibrium, and the number density (for a comoving volume) becomes "frozen." The present relic density is then approximately given by (28, 29)

$$\Omega_\chi h^2 \simeq \frac{T_0^3}{M_{\rm Pl}\langle\sigma_A v\rangle} \simeq \frac{0.1\,{\rm pb}\,c}{\langle\sigma_A v\rangle}.$$

Here σ_A is the total annihilation cross section of the WIMPs, v is the relative velocity of the WIMPs, and $\langle\cdots\rangle$ represents an average over the thermal distribution of WIMP velocities; T_0 is the equilibrium temperature, $M_{\rm Pl}$ is the Planck mass, and c is the speed of light. The freeze-out occurs at a temperature $T \simeq m_\chi/20$ almost independent of the properties of the WIMP, so they are already nonrelativistic when they decouple. A cosmologically interesting density arises for an annihilation of the order of the electroweak scale interaction. This last coincidence, which is not tuned, but comes directly from reliable calculations, represents one of the main motivations for believing that WIMPs could provide the dominant contribution to the matter in the universe. It is also important to note that smaller annihilation cross sections correspond to larger relic densities. WIMPs with stronger interactions remain in equilibrium for a longer time and hence decouple when the universe is colder, and so they are suppressed by a smaller Boltzmann factor.

A heavy neutrino would seem a very natural WIMP candidate. Calculations of its relic density show that for a Dirac neutrino it would provide $\Omega_\nu \sim 0.3$ for masses in bands around a few eV, a few GeV, or even a TeV. For masses smaller than $\sim$1 eV, and between $\sim$10 GeV to $\sim$100 GeV, the neutrino would have a very low abundance and be a subdominant DM component. For other ranges, it would over-close the universe and so is already excluded. As discussed above, a neutrino of mass $\sim$1 eV would be hot DM, and so is limited by structure formation considerations. LEP data exclude a fourth-generation heavy neutrino lighter than 45 GeV because of the absence of its contributions to the Z-decay width (30). In addition, it is one of the triumphs of early DM direct detection searches that Dirac neutrinos (heavier than $\sim$0.5 GeV), whose interaction cross section with target

nuclei is relatively large, were excluded as a dominant component of the galactic dark halo. Cosmions (106), another CDM candidate, were also ruled out both by their absence in direct search data and also by following the resolution of the solar neutrino problem.

The currently best-motivated WIMP candidate is the lightest superparticle (LSP) in SUSY models. These models are discussed in detail in the next section and are only summarized here. Stability of the LSP is ensured if the model conserves R-parity, a new quantum number, which distinguishes SUSY particles from "normal" matter. In conventional models, there are two candidates among the superparticles for CDM, the neutralino and the sneutrino. Sneutrinos have large annihilation cross sections that require a mass exceeding several hundred GeV for the predicted Ω_χ to be cosmologically interesting. This sits uncomfortably with the requirement that the sneutrino also be the lightest superparticle, since naturalness arguments (see below) would prefer a lighter LSP. In addition, existing WIMP searches rule out "ordinary" sneutrinos. The neutralino is much more strongly favored; calculations show that in a broad range of SUSY models it occurs as the LSP and would have the cosmologically required relic density.

Although the neutralino as LSP is undoubtedly the most popular WIMP candidate, a large range of nucleon-WIMP cross sections are allowed in this model. In the past couple of years, experiments such as WMAP and $g_\mu - 2$ have begun to place significant constraints on the possible cross sections, but the story is far from over. In order to make useful predictions from SUSY, considerable constraints and/or assumptions must be made to avoid dealing with over a hundred free parameters in the theory. The most popular constrained models, such as the minimal supergravity model (mSUGRA), are suffering increasingly from a problem of fine tuning, as their parameter space shrinks but no WIMP is observed. It may turn out that nature does not choose any of the currently popular models, but what makes SUSY so compelling as the source of a WIMP candidate is that in almost all the SUSY parameter space, a suitable DM candidate can be found.

The existence of axions was first postulated to solve the strong *CP* problem of QCD (31), and they also occur naturally in superstring theories (32). Axions are pseudo-Nambu-Goldstone bosons associated with the spontaneous breaking of a new global Peccei-Quinn (PQ) U(1) symmetry at scale f_α. Although very light, axions would constitute CDM, since they were produced by a nonthermal process of misalignment in the early universe. Their cosmological abundance can be calculated and requires a mass, $m_a \sim (10^7\,\mathrm{GeV}/f_a)\,\mathrm{eV} \sim (10^{-6}\text{–}10^{-4})$ eV for $\Omega_\mathrm{a} \sim 1$. Its interaction with ordinary matter is suppressed by the PQ scale $\sim(m_{\mathrm{W}/f_a})^2\sigma_\mathrm{EW} \sim 10^{-18}\sigma_\mathrm{EW}$ (where $\sigma_\mathrm{EW} \sim 10^{-2}$ pb is the characteristic electroweak cross section), which is extremely small.

A number of other proposed candidates are hypothetical solutions to the CDM problem. In many cases, they represent extremely elegant ideas and are consistent with current experimental constraints. However, there may be little else to currently motivate them as "natural" solutions. Only time will tell. Under SUSY, the axion has its fermionic superpartner, called the axino. Its mass is strongly

model-dependent, but in contrast to the neutralino, it is often not determined by the SUSY-breaking scale, $\sim$1 TeV. Hence the axino could be light, and would naturally be the LSP. Axinos could be warm DM (with masses $<$2 keV) (33), or more massive axinos could contribute directly to CDM (34, 35). WIMPZILLAs (36, 37) are very massive relics from the Big Bang, which can be DM in the universe if their mass is $\sim 10^{13}$ GeV. They could be produced at the end of inflation through a variety of possible mechanisms: gravitationally, during preheating, during reheating, or in bubble collisions. If they decay (albeit with a lifetime comparable to the age of the universe), then they may give rise to high-energy cosmic rays. Solutions using primordial black holes, which must have formed before the era of BBN, require a fair amount of fine tuning (38) so that they possess the properties to contribute to the CDM, rather than being counted in the baryonic DM component. Work on models in extra dimensions has given rise to some interesting CDM candidates, including a Kaluza-Kline graviton (39), although it may only be detectable through signatures in the CMB or large-scale structure.

Further references and some historical perspective are available in excellent theoretical reviews of DM candidates ((40–44); also see http://pdg.lbl.gov).

1.3. Further Discussion of SUSY Theoretical Models for WIMPs

SUSY is a new symmetry of space-time that has been discovered in the process of unifying the fundamental forces of nature (electroweak, strong, and gravitation). SUSY helps in stabilizing the masses of fundamental scalar particles in the theory, such as the Higgs boson. This is known as the hierarchy problem, which helps to explain why gravity is so much weaker than the other forces. SUSY requires the existence of a new particle for each particle in the standard model. The SUSY partners differ by half a unit of spin, and use the names sleptons (partners of leptons), squarks (partners of quarks), gauginos (partners of gauge bosons), and higgsinos (partners of Higgs bosons). Sleptons and squarks have spin 0, and gauginos and higgsinos have spin $\frac{1}{2}$.

If SUSY were an explicit symmetry of nature, superpartners would have the same mass as their corresponding standard-model particles. However, no such particles have been observed. It is therefore assumed that SUSY, much like weak symmetry, is broken. Superpartners are much heavier than their normal counterparts, which explains why they have not been detected so far. The mechanism for SUSY breaking is not completely understood, and in practice it is implemented by a set of SUSY-breaking parameters that govern the values of the superpartner masses—the superpartner couplings are fixed by SUSY.

Goldberg (46) and Ellis et al. (47) first suggested that the neutral gauginos and the neutral higgsinos, which have the same quantum numbers, can mix together. This superposition is referred to as a neutralino, χ, and in many models is the LSP. The WIMP LSP candidate must be an electrically neutral particle with no strong interactions because no evidence for it has shown up bound in exotic

heavy isotopes. The LSP is stable in SUSY models where R-parity is conserved, and this condition is usually extended to the so-called minimal supersymmetric model (MSSM), in which the LSP is expected to be the lightest neutralino. This is particularly true when one constrains the soft supersymmetric mass breaking terms $m_{1/2}$ and m_0 to be universal at an input Grand Unified Theory (GUT) scale, which results in the constrained MSSM (CMSSM). The CMSSM model depends only on the following parameters: $m_{1/2}$, the universal gaugino mass at the GUT scale; m_0, the universal scalar mass at the GUT scale; $\tan\beta = \langle H_2\rangle/\langle H_1\rangle$, ratio of vacuum expectation values of Higgs fields, where $\langle H_2\rangle$ gives mass to the top quark and $\langle H_1\rangle$ gives mass to the down quark and the lepton; A_0, the universal trilinear coupling constant; and μ, the sign of the Higgs mixing parameter.

If the universe is populated with neutralinos, it should be possible to detect their presence either directly, via inelastic collisions with nucleons, or indirectly, by observing the fermion-antifermion pairs that result when neutralinos annihilate. The expected cross sections of such interactions are determined by the allowed regions of parameter space in the SUSY model being used. Recent experimental results, most notably those from the WMAP satellite (16, 24), have further refined the allowed parameter space of the CMSSM. The WMAP result of $0.094 < \Omega_\chi h^2 < 0.129$, in particular, significantly restricts the allowed regions of the $m_{1/2}$, m_0 plane; indeed, it reduces the uncertainty in these values by a factor of four (48). For example, since $\Omega_\chi h^2 \propto m_\chi\, n_\chi$, where n_χ is the LSP relic density and m_χ the neutralino mass, one would expect the upper limit on m_χ to decrease when the upper limit on $\Omega_\chi h^2$ is decreased.

Figure 5 (see color insert; reproduced from Reference (49)) shows the allowed regions of the CMSSM parameter space for various values of $\tan\beta$ and μ.

The constraint from the WMAP $\Omega_\chi h^2$ value forces the allowed parameter space into two distinct branches, while the bulk region at the intersection of these branches is reduced to a very small area. This is a little alarming in that the bulk region was originally the favored region, but its exclusion is probably due to the CMSSM being essentially an overconstrained model. Further constraints from $b \to s\gamma$ (50, 51), $B_s^0 \to \mu^+\mu^-$ (52, 53), and the LEP light Higgs mass bound $m_h > 114.1$ GeV (54) prohibit much of the bulk region that was previously allowed. The Higgs mass bound is particularly relevant because in the CMSSM, the lightest SUSY Higgs boson is almost always standard-model-like (55).

An upper bound of 500 GeV on m_χ is now well motivated for $\tan\beta < 40$ (56), increasing the likelihood of detection at accelerators such as the LHC. Including the most recent $g_\mu - 2$ result (57) reduces the upper bound to 400 GeV. These data also force the range of $m_{1/2}$ to a much reduced value for fixed $\tan\beta$, although there is no change in the lower bound of $m_{1/2}$. A lower bound on m_χ is set to 108 GeV (irrespective of $g_\mu - 2$) for all values of $\tan\beta$, with the minimum occuring around $\tan\beta = 23$.

The most recent $g_\mu - 2$ value would severely limit the CMSSM parameters, mainly by forcing allowed values of $m_{1/2}$, m_0 (for $\mu > 0$ only) down to the lower end of both branches (the co-annihilation "tail" and rapid-annihilation "funnel").

The $\mu < 0$ case is disfavored by this result, especially when e^+e^- and τ-data are considered (58).

In the future, as the WMAP and Planck results further refine the measurement of $\Omega_\chi h^2$, we will see the values of m_0 and $m_{1/2}$ becoming more refined in turn (although the detection cross sections will not be affected (58)). At present, the value of m_0 is almost uniquely defined by the WMAP $\Omega_\chi h^2$ result in terms of the other CMSSM parameters. It would be, in principle, possible to fix $\tan\beta$ with accuracy $\Delta(\tan\beta) \leq 1$, if m_0 could be determined with an accuracy $\Delta(m_0) \leq 5$ GeV (the required accuracy in $m_{1/2}$ is very small because the allowed regions are nearly horizontal). It should be noted, however, that the value of $\tan\beta$ (for fixed $m_{1/2}$, m_0) has little effect on direct neutralino detection in DM experiments (49).

We now discuss other SUSY models that provide a natural DM candidate and are particularly attractive from a theoretical standpoint. The class of scenarios known as Yukawa unified models unify all matter of a single generation into a single 16-dimensional spinorial multiplet of SO(10) (58). The Higgs doublets are typically expressed in a 10-dimensional representation and $\tan\beta$ is typically large in this theory ($>$40), often resulting in a rather involved analysis. Yukawa unified models predict spin-independent neutralino-proton cross sections of the order 10^{-44} to 10^{-52} cm^2, i.e., the vast majority of the parameter space lies significantly below the reach of current direct detection experiments (55).

Another interesting group of SUSY GUTs are those formulated in extra dimensions (59–61). Gaugino-mediated SUSY breaking represents a subclass of these GUTs that are motivated by the brane-world scenario (62). One of the main features of these models is that the sfermion masses are loop-suppressed relative to the gaugino masses and can effectively be taken to be zero. The predicted spin-independent neutralino-proton cross sections are typically of the order 10^{-42} to 10^{-47} cm^2, although imposing the WMAP constraint $0.094 < \Omega_\chi h^2 < 0.129$ leaves only allowed regions with neutralino masses of 1200–2000 GeV (55).

Figure 4 (see color insert) shows a limited selection of the current theoretical predictions that are being tested, or will be tested in this decade, for SUSY WIMP direct detection experiments in the m_χ-σ_χ^{SI} plane.

2. DARK MATTER DIRECT DETECTION RATES

2.1. WIMP Signatures in Experiments

Heavy-particle DM can be looked for either through direct observation of nuclear recoils in terrestrial detectors or indirectly via the observation of their annihilation products, such as high-energy neutrinos, charged leptons, or gammas, whose sources include the sun, Earth, galactic halos, and the galactic center. The indirect methods can provide significant limits on WIMP properties, or in some cases possible evidence for WIMP detection. However, there are significant model dependencies in the predicted signals, and in general it is required that either they

are self-conjugate particles or both particle and antiparticle DM is available in sufficient abundance. Indirect detection rates and experimental data are discussed elsewhere (29, 42, 70–77) and are not covered further here.

The calculation of the WIMP direct detection rate in terrestrial detectors depends on several factors, which include the local halo density and velocity distribution in the Milky Way, the WIMP mass, and the cross section on the target nuclei. The last of these parameters has the largest uncertainty. SUSY-based calculations for neutralinos show at least five orders of magnitude variation in the nucleon coupling, and in some special cases the cross section can vanish. However, most models predict rates that are being tested either in existing experiments or in experiments that can be built in the next 10 years. The WIMP annihilation cross section is well constrained by the required Ω_χ. However, since the neutralino can annihilate into many possible particles, but the scattering cross section on nuclear targets is determined only by its coupling to quarks, a simple crossing symmetry argument provides only an upper limit on the direct-detection cross section.

Details of WIMP interaction-rate calculations can be found in References (29, 79, 81) and also in a number of the theory papers discussed in Section 1.3. Generally, the recoil energy spectrum is given by

$$\frac{dN}{dE_r} = \frac{\sigma_0 \rho_\chi}{2\mu^2 m_\chi} F^2(q) \int_{v_{\min}}^{v_{\rm esc}} \frac{f(v)}{v} dv,$$

where ρ_χ is the local WIMP density, μ is the WIMP-nucleus reduced mass $m_\chi m_N/(m_\chi + m_N)$ (assuming a target nucleus mass m_N), and the integral takes account of the velocity distribution $f(v)$ of WIMPs in the halo. The term $v_{\min}$ is the minimum WIMP velocity able to generate a recoil energy of E_r, and $v_{\rm esc}$ is the maximum WIMP velocity set by the escape velocity in the halo model. $F(q)^2$ is the nuclear form factor and σ_0 the WIMP nucleus interaction cross section, both of which will now be discussed in more detail.

The WIMP-nucleus cross section can have both spin-independent and spin-dependent components. For the former, the interaction will be coherent across the nucleons in the nucleus, whereas the latter term will only be present for nucleons with nuclear spin (29, 82, 83). In most cases, the coherent term will dominate because it has an A^2 enhancement (A, atomic number of nucleus); however, neutralinos with dominantly gaugino or higgsino states may only couple through the spin-dependent term. As the recoil energy rises, account must also be taken of the nuclear form factor, which for larger nuclei may suppress the differential scattering rate significantly.

These points can be best illustrated by showing the results (Figure 6) of a full calculation assuming the spin-independent coupling dominates, using standard halo parameters and the formalism discussed in Reference (81). A WIMP mass of 100 GeV is chosen with a cross section normalized to that for a single nucleon, which is representative of the best current limits in direct detection experiments (84). The figure shows both the differential and integrated (above the indicated threshold) WIMP event rate in $keV_{\rm r}$ expected for single isotope targets of ^{131}Xe (similar for

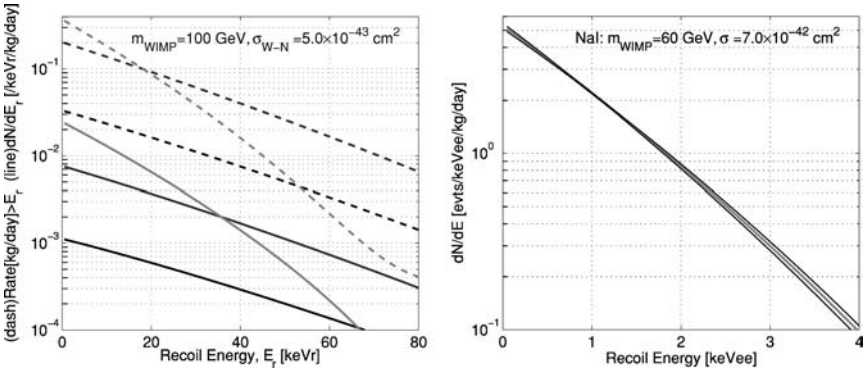

Figure 6 Left: Calculated differential spectrum in evts/keV/kg/d (lines), and the integrated event rate evts/kg/d (dashed lines) above a given threshold energy (keV_r), for Xe, Ge, and S targets (light to dark). A 100 GeV WIMP with a spin-independent cross section for WIMP-nucleon of $\sigma = 5 \times 10^{-43}$ cm^2 has been used. Right: The differential spectrum for NaI (black line) in evts/keVee/kg/d (see Section 2.2 for a discussion of units) for a 60 GeV WIMP with a spin-independent cross section for WIMP-nucleon of $\sigma = 7 \times 10^{-42}$ cm^2 (dominated by I recoils). The spread of the lines above and below indicate the change in the recoil spectrum expected, under standard halo assumptions, for June (upper line at high energy, lower line at low energy) and December. The energy scale is in keV_{ee} assuming a quenching factor of 9% I recoils). The amplitude of the annual modulation of the WIMP signal (without additional background) in the 2–4 keV_{ee} bin is 4.2% of the average count rate in that energy range.

^{129}I), ^{73}Ge, and ^{32}S (^{28}Si would have a curve 20% below that of ^{3}2S). It can be seen that for a given interaction cross section for WIMP-nucleon interactions, the smaller nuclei are penalized owing to a combination of smaller coherence enhancement ($\sim A^2$) and the less effective transfer of recoil energy to a target that is lighter than the WIMP. The recoil spectrum for the heavier Xe nucleus is significantly suppressed by the loss of coherence for higher q^2 scattering events (form factor suppression). For a 100 GeV WIMP, the integrated event rate drops by a factor of two for a threshold recoil energy increase of 13, 20, and 22 keV_r for Xe, Ge, and S respectively. A low analysis threshold is therefore important to maximize the effective search sensitivity of a given nominal detector mass. The influence of threshold energy is even greater for lower-mass WIMPs, where the recoil spectrum slope becomes steeper because of the reduction in typical kinetic energy of the WIMPs.

In the absence of backgrounds, the search sensitivity of a detector array is directly proportional to the mass (M) $\times$ exposure time (T) as any hint of a DM recoil spectrum is looked for. In a mode where subtraction of an estimated background becomes necessary, the sensitivity improvement becomes proportional to $\sqrt{MT}$ (85). Ultimately, the subtraction becomes limited by the systematics of calibrating the detector response to the background, and no further improvement in sensitivity is possible.

In order to compare results from different direct search experiments, it is usual to renormalize the cross section on the target nucleus (or nucleii) to the equivalent cross section on a single nucleon. This requires the assumption of either spin-independent or spin-dependent coupling calculations discussed above. It should also be noted that the differences in the reduced mass for different nuclear targets are allowed for by also normalizing to the reduced mass of a single nucleon. What is typically plotted is the single nucleon-WIMP equivalent cross section versus WIMP mass (see examples in Figures 7 and 4).

2.2. Quenching Factors and Discrimination

Detectors respond differently to nuclear recoils than to electron recoils. The term quenching factor is used to describe the difference in the amount of visible, or measurable, energy in a detector for these two classes of events. The dominant backgrounds typically arise from gamma rays and x-rays, which deposit energy via electron recoils. Neutrons and WIMPs will deposit energy via nuclear recoils. In a generally accepted notation in the field, $keV_{\rm ee}$ is used to quantify a measured signal from the detector in terms of the energy of an electron recoil that would be required to generate it. $keV_{\rm r}$ is used similarly for a nuclear recoil event. If a particular detection mechanism has a quenching factor QF, it then holds that for a nuclear recoil event of energy E_r, the electron recoil event that would produce an equivalent signal is given by

$$E_e(keV_{\rm ee}) = QF \times E_r(keV_{\rm r}).$$

The energy scale for $keV_{\rm ee}$ can be established with gamma line sources (and also lines arising from internal radioactivity in the detectors). The nuclear recoil response can be established using neutrons (rather than WIMPs), either in a neutron scattering experiment where the energy of the incoming neutron is well defined and its angle of scattering measured, or by using a neutron source with a broad energy distribution, and comparing the observed shape of the nuclear recoil spectrum with detailed Monte Carlo simulations. In addition, the observation of events arising from the recoil of the daughter nucleus from an alpha decay at the surface of a detector can also be used to verify the energy response of detector to a nuclear recoil events.

For many experiments that use more than one detection mechanism simultaneously, the fact that the quenching factors are different for two different detection mechanisms allows them to distinguish between nuclear and electron recoil events. This discrimination is key to driving down the effective backgrounds to allow the observation of WIMP nuclear recoil events. Various examples of this are given in the following sections.

2.2.1. ANNUAL MODULATION AND DIRECTIONALITY

Annual modulation of the WIMP signal was first discussed in References (86–88). It arises because the

velocity of a DM detector through the WIMP halo changes as the Earth moves around the sun. The magnitude of the net velocity peaks around June 2 ($v \sim 245$ km/s) with a minimum six months later ($v \sim 215$ km/s). The details of the appropriate calculations can be found in References (29, 81, 88–90), but to illustrate the magnitude of the effect, the variation in the expected WIMP recoil spectrum for the case of the signal that would be observed in the DAMA NaI experiment is shown in the right-hand plot of Figure 6. The calculations assume as a reference model a simple isothermal halo model with a velocity dispersion of 220 km/s. Because the effect is subtle ($\sim$5% variation in the event rate), a large number of WIMP events must occur in a detector for the effect to be measurable statistically. Experiments that seek to observe annual modulation require a much larger detector than those intended to identify a limited number of individual WIMP recoil events. Also, it is necessary to distinguish between observed annual modulation and modulation in backgrounds or other possible systematics.

For a given combination of WIMP velocity, WIMP mass, and target nucleon mass, the modulation shows a pivot point around which the phase of the annual modulation is reversed. Observation of this feature would provide significant additional evidence for the existence of a WIMP signal in a detector. Unfortunately, its observation requires a low energy threshold and may be out of reach for many experiments.

Naturally, there has been some discussion of the velocity distribution function of the particles that populate the dark halo, with more complex models ranging from spherically symmetric to triaxial to discontinuous (including caustics). For isothermal models, it is typical to consider a range of velocity dispersions $v_0 =$ 170–270 km/s; the central value is the one most often used. This is discussed in greater detail in Section 5.1.

Because of the general motion of the sun through the WIMP halo (in a direction toward Cygnus), it is expected that the angular distribution of nuclear recoils from WIMPs will be significantly anisotropic (88, 90, 91). Confusion with any signal from a terrestrial background source is unlikely. At present, the gas-based detectors discussed in the next section are the only technology that can measure such an anisotropy, although they will measure the anistropy of the axis of the recoil (i.e. a front/side asymmetry) rather than being able to establish the direction of the recoil (front/back asymmetry). This reduces the statistical sensitivity of the search technique, but it would still provide very strong evidence that the signal is consistent with that originating from WIMP interactions.

3. PAST, PRESENT, AND FUTURE EXPERIMENTAL SEARCHES

This section summarizes some of the leading direct detection experiments that have searched, are searching, or will search for DM direct detection signals (see Tables 1–3). New detector technologies enable us to look for signatures

18 Aug 2004 18:39 AR AR228-NS54-10.tex AR228-NS54-10.sgm LaTeX2e(2002/01/18) P1: JRX

TABLE 1 Completed dark matter experiments (chronological)

Collaboration	Location	Readout	Target mass	Search dates
USC-PNL	Homestake (USA)	Ionization (77 K) $\beta\beta$	0.2 kg Ge	1986–
USCB-LBL	Oroville (USA)	Ionization (77 K) $\beta\beta$	0.2 kg Ge	1986–
ZAR-USC-PNL	Canfranc (Spain)	Ionization (77 K) $\beta\beta$	0.2 kg Ge	1986–
Caltech-PSI-Neuchatel	Gothard (Switzerland)	Ionization (77 K) $\beta\beta$	0.2 kg Ge	1986–
MIBETA	Gran Sasso (Italy)	Ionization (77 K) $\beta\beta$	$\sim$1 kg TeO_2	1988–
EDELWEISS-0	Fréjus (France)	Therm. phon. ($\sim$30 mK)	$\sim$0.1 kg Al_2O_3	1988–
Heidelberg-Moscow	Gran Sasso (Italy)	Ionization (77 K) $\beta\beta$	0.2–3 kg Ge	1990–
COSME	Canfranc (Spain)	Ionization (77 K)	0.2 kg Ge	1990–1992
NaI32 (ZAR)	Canfranc (Spain)	Scint. (300 K)	30 kg NaI	1992–1995
BPRS	Gran Sasso (Italy)/Fréjus (France)	Scint. ($\sim$300 K)	6 kg NaI	1992–94
Saclay-NaI	Fréjus (France)	Scint. ($\sim$300 K)	10 kg NaI	1997–
DEMOS	Sierra Grande (Argentina)	Ionization (77 K)	1 kg Ge	1994–1997
IGEX	Canfranc (Spain), Baksan (Russia)	Ionization (77 K) $\beta\beta$	6 kg Ge	1994–2000
CRESST I	Gran Sasso (Italy)	Therm. phon. ($\sim$10 mK)	$\sim$1 kg Al_2O_3	1995–2003

EDELWEISS I	Fréjus (France)	Therm. phon. + ioniz. (∼30 mK)	0.1 kg Ge	1995–1999
COSME II	Canfranc (Spain)	Ionization (77 K)	0.2 kg Ge	1998–2004
DAMA	Gran Sasso (Italy)	Scintillator (∼300 K)	≤100 kg NaI array, 10 kg CaF_2	1995–2002
ELEGANTS V	Otto-Cosmo (Japan)	Scintillator (∼300 K)	∼100 kg NaI array	1995–2000
DAMA-Xe	Gran Sasso (Italy)	Scintillator PSD (∼150 K)	6 kg Xe	1995–2002
UKDM–NaI	Boulby (UK)	Scintillator (∼300 K)	≤1–5 kg NaI	1996–2000
ELEGANTS VI	Otto-Cosmo (Japan)	Scintillator (∼300 K)	∼100 kg CaF_2 array	1996–
CDMS I	Stanford (USA)	Therm. phon. + ioniz. (∼20 mK)	∼1 kg Ge	1995–2001
		Non-therm. phon. + ioniz. (<50 mK)	∼0.1 kg Si	1997–2001
Rosebud	Canfranc (Spain)	Therm. phon. (∼20 mK)	0.1 kg Ge	1998–1999
IGEX–DM	Canfranc (Spain)	Ionization (77 K)	6 kg Ge	1999–2001
HDMS	Gran Sasso (Italy)	Ionization (77 K)	0.2 kg Ge (+ veto det.)	2000–2003
Tokyo-DM	Kamioke (Japan)	Therm. phon. (∼20 mK)	0.2 kg LiF	2001–2003
NaIAD	Boulby (UK)	Scintillator (∼300 K)	≤50 kg NaI array	2001–2003

TABLE 2 Current status of dark matter experiments (by technology)

Collaboration	Location	Readout	Target mass	Search dates
IGEX–DM	Baksan (Russia)	Ionization (77 K)	3 kg Ge	2001–
IGEX–DM	Canfranc (Spain)	Ionization (77 K)	2 kg Ge	2001–
GENIUS TF	Gran Sasso (Italy)	Ionization (77 K)	∼5 kg Ge $\beta\beta$	2002–2005
NAIAD	Boulby (UK)	Scintillator (∼300 K)	∼50 kg NaI array	2001–2005
LIBRA	Gran Sasso (Italy)	Scintillator (∼300 K)	≤250 kg NaI array	2003–
ANAIS	Canfranc (Spain)	Scintillator (∼300 K)	11 kg NaI prototype	2000–2005
Rosebud	Canfranc (Spain)	Therm. phon. (∼20 mK)	≤1 kg Ge, Al_2O_3	1995–
Rosebud	Canfranc (Spain)	Therm. phon. + scint. (∼20 mK)	∼1 kg $CaWO_4$, BGO	2000–
CDMS II	Soudan (USA)	Non-therm. phon. + ioniz. (<50 mK)	0.2–1.5 kg Si, 1–4.2 kg Ge	2001–2006
EDELWEISS II	Fréjus (France)	Therm. phon. + ioniz. (∼30 mK)	1 kg Ge	2000–2004
CRESST II	Gran Sasso (Italy)	Therm. phon. + scint. (∼10 mK)	1 kg $CaWO_4$	2000–2006
CUORICINO	Gran Sasso (Italy)	Therm. phon. (∼20 mK)	40 kg $T2O_2$ $\beta\beta$	2002–
ORPHEUS	Bern (Switzerland)	Superconducting grains (∼4 K)	0.5 kg Sn	2001–
SIMPLE	Rustrel (France)	Superheated droplets (∼300 K)	Freon	1999–
PICASSO	Sudbury (Canada)	Superheated droplets (∼300 K)	∼10 g–1 kg Freon	2001–
ZEPLIN I	Boulby (UK)	Scintillator PSD (∼150 K)	6 kg LXe	2002–2004
XMASS-DM	Kamioke (Japan)	Scint. + ioniz. (∼150 K)	2 kg LXe	2002–2004
XMASS-DM	Kamioke (Japan)	Scint. + ioniz. (∼150 K)	14 kg LXe	2004–
DRIFT–I	Boulby (UK)	ioniz. NITPC (300 K)	0.167 kg CS_2	2002–2005
Bubble Chamber (Chicago)	Soudan (USA)	Superheated liquid (∼300 K)	1 kg Freons	2004–
(MACHe3)	Grenoble (France)—not underground	Exciton (∼20 mK)	0.02 g He_3	1998–

TABLE 3 Future dark matter experiments

Collaboration	Possible location	Readout	Max target mass	Planned search
GEDEON	Canfranc (Spain)	Ionization ($\sim$77 K) $\beta\beta$	60 kg Ge	2006–
GENIUS	Gran Sasso (Italy)	Ionization (77 K) $\beta\beta$	$\sim$100 kg Ge	2006–
MAJORANA	tbd	Ionization (77 K) $\beta\beta$	$\sim$100 kg Ge	2005–
ANAIS	Canfranc (Spain)	Scintillator ($\sim$300 K)	107 kg NaI array	2006–
CDMS III	Soudan (USA)	Non-therm. phon. + ioniz. (<0.1 K)	1.5 kg Si 4.2 kg Ge	2006–
CryoArray	(tbd)	Non-therm. phon. + ioniz. (<0.1 K)	100 kg–1000 kg Ge	2008–
EDELWEISS II	Fréjus (France)	Therm. phon. + ioniz. ($\sim$30 mK)	12 kg Ge	2005–
CRESST III	Gran Sasso (Italy)	Therm. phon. + scint. ($\sim$10 mK)	10 kg $CaWO_4$	2005–
CUORE	Gran Sasso (Italy)	Therm. phon. ($\sim$20 mK) $\beta\beta$	760 kg TeO_2	2005–
ZEPLIN II	Boulby (UK)	Scint. + ioniz. ($\sim$150 K)	30 kg LXe	2004–
ZEPLIN III	Boulby (UK)	Scint. + ioniz. ($\sim$150 K)	7 kg LXe	2004–
ZEPLIN–MAX	Boulby (UK)	Scint. + ioniz. ($\sim$150 K)	100–1000 kg LXe	2007–
XMASS-DM	Kamioke (Japan)	Scint. + ioniz. ($\sim$150 K)	100–1000 kg LXe	2006–
XENON10	(tbd)	Scint. + ioniz. ($\sim$150 K)	10 kg LXe	2005–
XENON100	(tbd)	Scint. + ioniz. ($\sim$150 K)	100–1000 kg LXe	2007–
DRIFT–10	Boulby (UK)	ioniz. NITPC (300 K)	2 kg CS_2/Xe	2006–

associated with WIMP recoils, such as an annual modulation of the recoil spectrum, or to observe directional anisotropy of the recoils. Many detectors can distinguish nuclear recoil events, which arise from direct WIMP interactions, from electron recoils that arise from the majority of backgrounds. Other technologies drive down the raw level of competing backgrounds to gain a superior sensitivity.

Given the scientific importance of the problem of DM and the search for SUSY, a reasonably broad portfolio of complementary experiments will be essential. Different technologies, reaching eventually similar sensitivities, will tend to have different systematics and provide critical cross checks for a detection claim, and will then permit extraction of physics parameters.

As a general point, the sensitivity of DM experiments clearly scales with mass. However, the sensitivity often becomes limited by systematics, which frequently scale with the active surface area.

3.1. The Rate of Change of Progress

We should review the past, in order to consider how robust our future predictions might be. Figure 1 shows the time development of the best scalar WIMP-nucleon σ limit from the mid 1980s to the present. The first decade was dominated by conventional high-purity Ge (and Si) semiconductor ionization detectors. The design of these detectors was to some extent "off-the-shelf," and progress was achieved, for the most part, by allowing the cosmogenic activation of the detectors to cool, and also by improving the low background shielding around the detectors. In the mid 1990s, results from NaI scintillator detectors became competitive. These detectors used pulse shape discrimination (PSD) to make statistical distinctions between populations of electron recoil events and nuclear recoil events. In principle, the intrinsic background of the detector and environment were no longer the limiting factors, since with sufficient exposure time and target mass the limits could be driven down. However, the relatively poor quality of the NaI discrimination meant that systematic effects rapidly dominated, halting any further improvement of mass $\times$ time. The NaI detector technology could also be described as off-the-shelf, but the low background and high-light-yield housing systems were definitely novel. In the case of the DAMA experiment, the deployment of an $\sim$100 kg array of NaI also allowed the search for a WIMP annual modulation signal. At the end of the 1990s, new detector technology (in the form of cryogenic detectors) that had been developed specifically for direct detection finally took the lead in terms of sensitivity.

If we now look forward at some of the goals of a few experiments over the next decade, it is immediately apparent that the forecast rate of progress is rapidly accelerating. The question is whether this is simply a "triumph of hope over expectation" or represents a genuinely improved rate of progress that stems from applying new detector technologies (e.g., two-phase Xe, semiconductor, and scintillator cryogenic detectors, naked HPGe) that were "birthed" with this specific application in mind.

Large-mass cryogenic detector technology has clearly reached a level of maturity within the field of DM direct detection and also for double-beta decay ($\beta\beta$–decay) experiments. Detector arrays have been operated in underground sites by a number of groups worldwide for >5 years. The technical challenges associated with long-term operation of large detectors at temperatures <100 mK are being met. The original technical motivation for deploying cryogenic detectors in the search for DM is as strong as ever. The identification of candidate WIMP recoil events (the majority of which are expected at energies 0–30 $keV_{\rm r}$) is much enhanced by the ability to measure the recoil energy on an event-by-event basis and the ability to determine unambiguously the nature of the recoil interaction (i.e., nuclear recoil versus electron recoil). The discrimination is significantly enhanced by the excellent signal-to-noise ratio possible in cryogenic detectors, where noise contributions of $\sim 1\ keV_{\rm vis}$ are routinely achieved.

In comparison, experiments based on liquid Xe, liquid Ar, and liquid Ne are working with a smaller number of detected quanta, such that the energy resolution in the expected WIMP recoil energy region is typically dominated by Poisson statistics. It is relatively early in the development cycle of these detectors, and their operation in deep underground sites has only just begun. The advantage of this type of technology is that, once prototypes have demonstrated the capacity to clearly discriminate electromagnetic backgrounds at the >99% level and to unambiguously identify WIMP nuclear recoils, they will be able to scale rapidly in size to 1 tonne. Some lessons can be taken directly from the high-energy physics community, although it should be emphasized that the energy thresholds required are somewhat lower than that typical for accelerator and neutrino beam targets.

The gas-based detectors are an interesting technology, which could be used, in the event of a WIMP discovery, to test the momentum vector distribution of the WIMPs in the Milky Way halo. However, the limited target mass that is currently realizable, especially when compared to the continuing improvements in the target masses of the solid/liquid-based experiments, means that an initial discovery is unlikely using this technology.

The proposed use of naked HPGe ionization detectors in liquid N_2 is innovative, and they may be relatively simple to deploy. However, if such a system is to be used to probe $\sigma \sim 10^{-45}$ cm^2, this would require $\sim 3 \times 10^3$ reduction in the low-energy gamma/beta backgrounds of the detector assembly compared to the current Ge detector levels, since the detector has no background discrimination. Low energy ($E < 100$ keV) backgrounds are very difficult to simulate reliably because the observed rate will probably be limited by small localized contamination rather than by distributed levels of U/Th/K.

Recent additional experimental reviews of WIMP direct detection are available (92, 93). The following sections describe a limited selection of experiments in some detail in order to compare their strengths and weaknesses (Figure 7 shows results from several experiments). As a consequence of this strategy, there are a number of other DM detector experiments to which this review cannot do justice. They include the CUORE experiment (94), the ORPHEUS experiment based on superconducting tin grains (95), the ROSEBUD experiment (96, 97), the

LiF-Kamioke experiment (98), and a possible technology employing superfluid ^{3}He (99).

3.2. Ionization Detectors

Experiments based on Ge ionization detectors, which had started in the late 1980s to look for neutrinoless $\beta\beta$–decay of ^{76}Ge, were also able to be used for DM searches (100–105). The $\beta\beta$–decay signal was being looked for at $\sim$2 MeV, whereas the DM recoil would occur at the lowest energies. It should be remembered that because nuclear recoils are 25% quenched relative to electron recoils in the Ge ionization signal, an observed energy of say 5 keV_{ee} in the detector corresponds to a WIMP recoil of $\sim$20 keV_r. The WIMP sensitivity of the detectors was limited by the absolute level of low-energy background (since no additional discrimination was possible), and the energy threshold was limited by electronics noise. In the early experiments, backgrounds were reduced somewhat by improvements in shielding but primarily by the cooling of the cosmogenically induced radioactive backgrounds over time as the detectors remained underground. Ionization detectors based on Si were also employed in direct searches for low-mass WIMPs, where the recoil kinematics are more favorable (106). The ionization detectors played an important role in eliminating both Dirac neutrinos and cosmions as possible DM candidates.

Future Ge-based $\beta\beta$–decay experiments [including MAJORANA (107), GENIUS (108), and GEDEON (92)] intend to scale in mass to $\sim$500 kg, with a significant reduction in backgrounds, through a combination of novel shielding, ultrapure materials selection, and production of detectors underground to reduce cosmogenic contributions. Smaller prototypes of these experiments are under construction or are now operating. The low-energy backgrounds relevant for DM searches will benefit significantly from the reduction in the Compton tail contribution from the higher-energy gammas that are the main concern for the $\beta\beta$–decay signal searches. Cosmogenically produced tritium in the Ge is of particular concern for DM sensitivity because the endpoint of its beta-decay spectrum is 18.6 keV_{ee} ($\sim$75 keV_r) and so spans the entire range of the expected DM recoil signal. At sea level, tritium is estimated to be produced in Ge at a rate of $\sim$100 atoms/kg/d. Only 100 atoms of tritium would lead to a decay rate of $\sim$0.015 evts/d, so this isotope is a significant consideration for future DM sensitivity in the absence of additional background discrimination. The desire to avoid the contribution of tritium and other cosmogenic isotopes (e.g., ^{68}Ge) to the low-energy spectrum will strongly favor underground production of detectors.

The large mass of the Ge $\beta\beta$–decay arrays will also allow them to make direct searches for annual modulation evidence, which will extend to a sensitivity at least two orders of magnitude below that of the current DAMA annual modulation signal.

3.3. Solid Scintillation Detectors: NaI/CsI

Results from NaI detectors for DM detection began appearing in the mid 1990s. These detectors were eventually able to set direct detection sensitivity limits beyond

those of the Ge and Si ionization detectors. Although the raw gamma backgrounds of the NaI detectors were worse than those of the Ge detectors, the sensitivity of the NaI detectors was enhanced because the nuclear recoil populations could be statistically distinguished from electron recoils using the pulse shaped discrimination (PSD). At low energies, below 30 keV_{ee}, the time-constant distributions of the two types of recoil overlap, and so individual pulses can no longer be uniquely assigned to one type or the other. However, the overall distribution of time constants during a WIMP search can be compared to the expected distributions from gamma (electron recoil) and neutron (nuclear recoil) calibrations, and a statistical estimate of the component of possible WIMP (nuclear recoil) events be made. Again it should be borne in in mind that the quenching factor in NaI scintillators is 30% and 9% for Na and I nuclear recoils respectively, which means, for example, that the scintillation light from a 22 keV_r WIMP recoil on I is equivalent to that from a 2 keV_{ee} electron recoil.

Preliminary NaI results were reported by the BPRS (Beijing-Paris-Roma-Saclay) Collaboration (half of the members of which also form the DAMA Collaboration) operating detectors at Gran Sasso, Modane, and Mentogou (109, 110). Then a series of improved DM limits from NaI using PSD were published by BPRS (111), DAMA (112) at Gran Sasso, ELEGANTS (113, 114) at Osaka, and the Boulby DM collaboration (115, 116).

The DM collaboration at Boulby Mine operated a range of NaI crystals underground from 1994 to 2004. In 1995, the collaboration reported results from the operation of a 1.3 kg NaI crystal (115). These results showed an improved sensitivity for spin-independent WIMPs that was three times better than the existing spin-dependent limits from underground Ge detectors, and was similar to that of the ELEGANTS and BPRS groups at that time. In 1996 (116) the collaboration reported results from the operation for 6 months of a 6 kg NaI crystal using PSD over an energy range of 4–25 keV_{ee}. This run achieved a much improved sensitivity to nuclear recoils that was a factor of 10–30 below the gamma and beta background. The photomultiplier tube (PMT) signals were typically 3–6 photoelectrons per keV_{ee} deposited in the NaI. These results showed a slightly better sensitivity to spin-independent WIMPs than that from the Ge ionization detectors, and a 50-fold improvement in spin-dependent limits. (Note that at this time, for spin-independent limits, the collaboration was using a nucleus-to-nucleon normalization that was based on the number of neutrons, rather than nucleons, squared. This means that the actual cross-section limits need to be rescaled when compared with other plots.) There was considerable optimism at that time that these sensitivities from NaI could be further improved by a factor of 10–100.

In 1996 the DAMA Collaboration reported (112) new results from a large NaI array [4×7.1 kg and 9×9.7 kg NaI(Tl)] using PSD. The data were analyzed with a software threshold of 2 keV_{ee}, although the background rejection using PSD only became effective above 4 keV_{ee}. The backgrounds were comparable to those of the Boulby experiment, but the light collection efficiency was better (5–7 photoelectrons/keV_{ee}) and a greater exposure was accumulated ($\sim$4100 kg–days), which enabled a fourfold improvement in the statistical limit.

At this point the DAMA array was repurposed for an annual modulation search. It was determined that the systematic uncertainties associated with PSD are too great to provide the underlying stability required for an annual modulation search, and no further results based on PSD were reported by DAMA. It should be noted that the final PSD result from DAMA (known as DAMA0) sets a 90% CL exclusion limit, which is a factor of two below the best fit to the annual modulation amplitude under standard halo assumptions.

The Boulby DM program continued to push the use of PSD to increase the sensitivity of the NaI detectors. In 1998 the Boulby and Saclay groups (117, 118) reported that improvement in sensitivity was being hampered by the observation of anomalous events in the background whose time constants were shorter than those expected for both electron events (majority of the signal) and nuclear recoil events. The energy spectrum of these events was too flat to be consistent with DM events. It was subsequently determined (see Reference (119) for review) that the anomalous events were arising from surface contamination of the crystals by an alpha-emitting isotope from Rn decay. The NAIAD (NaI Advanced Detector) program was implemented to study this problem and also to evaluate the use of unencapsulated NaI to further improve light yield and reduce background and surface contamination. In 2002 six NaI detectors with a total mass of 46 kg were running underground at Boulby. The latest results show that the unencapsulated detectors are free of the problem (120). The collaboration is, however, moving the majority of its resources to the liquid Xe program.

The larger masses of the NaI detectors permitted searches for annual modulation signals. The Zaragoza Collaboration, operating at Canfranc, Spain (121, 122), reported in 1996 no statistical evidence for annual modulation from a search that used 32 kg of NaI (without PSD) and operated over a period of two years, albeit with lower sensitivity and a higher threshold than those of the DAMA experiment that reported later.

In late 1997 (123) the DAMA Collaboration reported preliminary results indicating that a positive annual modulation signal was being observed in the lowest energy bins when $\sim$3400 kg–days taken in the winter were compared to $\sim$1200 kg–days taken the following summer. The DAMA experiment used for annual modulation consists of an array of nine NaI(Tl) crystals with a total mass of 100 kg, operated for a continuous seven-year period that ended in July 2002 (124). DAMA recorded an exposure of 108,000 kg–days and has reported an annually modulated $[A\cos(\omega[t - t_0])]$ variation in the signal, at 6.3σ CL, dominated by data from the lowest reported energy bins (2–4 keV_{ee}), shown in Figure 8. The time-averaged event rates across the array in the 2–3 keV_{ee} and 3–4 keV_{ee} bins after cuts and adjustment for efficiencies appear to be 1.0 evts/keV/kg/d and 1.9 evts/keV/kg/d, respectively. The best fit of the amplitude of the modulation is 0.023 ± 0.005 evts/keV/kg/d for 2–4 keV_{ee}, which is a fluctuation of $\sim\pm 1.6\%$ in the total count rate. Results are reported for the oscillation amplitude in integrated bins of 2–5 keV_{ee} and 2–6 keV_{ee}; however, the effect appears to be dominated by the behavior of the lowest energy bin range. These data have been analyzed in a

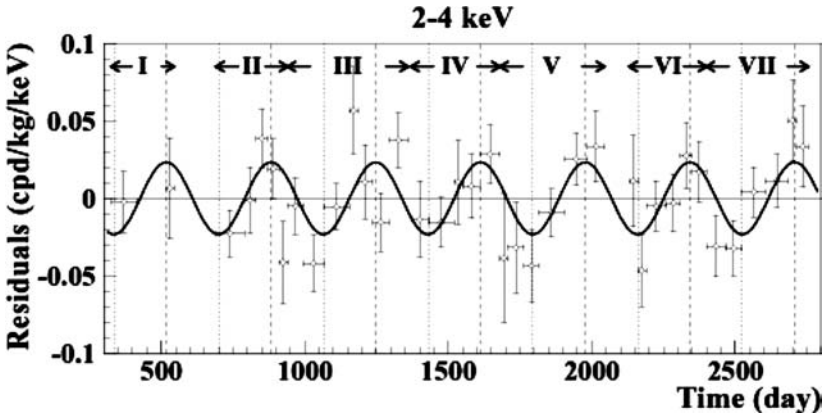

Figure 8 The DAMA annual modulation signal, showing the variation in count rate from the average over a seven-year data-taking period in a 2–4 keV_{ee} energy bin.

model-independent fashion using a simple cosine fit (125) and are in good agreement with previously reported results from earlier analysis of smaller exposures. Importantly, the authors state that the results are independent of the time binning used. The period of the oscillation is found to be 1.00 ± 0.01 y and the offset, t_0, is 140 ± 22 d with all parameters kept free in the fit. Now that the collaboration possesses such high statistics, it would be interesting to see the results of independent fits to the 2–3 keV_{ee} and 3–4 keV_{ee} binned data.

The DAMA array has been replaced by a new 250 kg NaI(Tl) array of ultra-radiopure crystals (LIBRA) in the same shielding enclosure at Gran Sasso, which began long-term data taking at the end of 2003. The projected backgrounds for LIBRA should be somewhat lower than those of the DAMA array, since both the PMTs and NaI crystals have been specially selected for reduced radioactivity. If the backgrounds are lower, this array should be able to rapidly confirm the annual modulation signal with much greater signal to noise and reduced systematics. In addition, if the software analysis threshold of the detector can be lowered below 2 keV_{ee}, it may be possible to observe the event rate both above and below the pivot point of the DM recoil spectrum. This would enable a more precise determination of the mass of the candidate WIMP as well as some cross check of possible systematic errors.

The Zaragosa group plans to construct a 100 kg NaI array (ANAIS) at the Canfranc Underground Laboratory [2450 meters water equivalent depth (mwe)] in Spain. This system will use NaI from a previous NaI array that has been underground since 1987. A prototype of ANAIS containing one of the array crystals has been operated (126) with an exposure of ∼2100 kg–days and a threshold of 4 keV_{ee}. The current limit curves are well above those of DAMA; however, the

18 Aug 2004 18:39 AR AR228-NS54-10.tex AR228-NS54-10.sgm LaTeX2e(2002/01/18) P1: JRX

intention is to construct a larger array and use a combination of annual modulation and PSD to push the sensitivity to a level that permits checking of the DAMA result.

3.4. Cryogenic Detectors: Sub-Kelvin

3.4.1. THERMAL PHONONS AND IONIZATION Since October 2002 the Edelweiss Collaboration (127, 128) has been operating 3 × 320 g Ge cryogenic detectors, operated at ∼25 mK, in the Laboratoire Souterrain de Modane Laboratory, Fréjus Tunnel (4000 mwe), on the France-Italy border. The technology uses neutron transmutation doped (NTD) Ge thermistors to read the thermal phonon signal (on time scales ∼100 ms) arising from particle interactions. An ionization signal from the Ge detectors (time scale ∼50 μs) is simultaneously measured for the particle event. When corrected for the Neganov-Luke effect (129), the phonon signal provides a direct measurement of the recoil energy for either electron or nuclear recoils. (No relative quenching is observed for nuclear versus electron recoils.) For the ionization measurement, nuclear recoils have a quenching factor of ∼25% relative to electron recoils. This difference in response for ionization versus phonon readout can be used to reject electron recoil events to better than 99.9% above a threshold of 20 keV_r.

The most recent published results of Edelweiss represent a total exposure of 30.5 net kg–days after cuts, summed from runs in the years 2000, 2002, and 2003. Their analysis uses a threshold of 20–30 keV_r (detector dependent). Relative to the CDMS (Cryogenic Dark Matter Search) experiment, described below, this elevated threshold decreases the sensitivity for the same nominal exposure. The data contained two nuclear recoil event candidates above threshold. Possible explanations for these events are that they arise from (α, n) neutrons from surrounding rock, penetrating the 20 cm polyethylene shield (this shield is now being upgraded), or that they result from leakage from the electron recoil band.

The collaboration has ceased running at Modane (March 2004) in order to install a much larger cryostat capable of running ∼30 kg of detectors. An upgrade to a 7 kg target mass has been approved, and new search runs are expected in 2005. The collaboration is also developing a new fast phonon readout scheme based on NbTi thin films. However, these devices have not yet been operated at Modane.

The initial phase of the CDMS experiment (CDMS I) was operated (1996–2002) at the Stanford Underground Facility (SUF) (130, 131). SUF has a muon flux only five times lower than that at the Earth's surface. CDMS I operated several 160 g Ge thermal phonon and ionization detectors of a similar design to those deployed by Edelweiss. During initial detector operation, electron recoil events at the surface of the detectors showed incomplete charge collection. This mimicked a reduced quenching factor, and a fraction of the electron recoil events were misidentified as nuclear recoil events. This leakage was significantly reduced by the introduction of new ionization contacts, which are formed by using a combination of Al Schottky contacts on a thin amorphous Si layer (132).

From 2000 to 2002, additional Ge and Si Z-dependent ionization and phonon (ZIP) detectors were also operated at this site (ZIP detectors are described in the next section). Results were reported for 119.1 live days of operation using four Ge ZIP and two Si ZIP detectors at the shallow site. WIMP search results from three Ge detectors of 89.3 raw kg–days (54.3 net kg–days after cuts) show 19 single-scatter events that pass the nuclear recoil maximum likelihood cuts. In addition, the detection of seven multiple-scatter neutron (nuclear recoil) events in this data set indicates an expected neutron single-scatter nuclear recoil background, so statistically nearly all of the 19 single-scatter nuclear recoil candidates can be due to neutrons. Further Monte Carlo studies have established that these neutrons arise from muon interactions in the rock. To overcome this irreducible background at the shallow site, the same tower of six ZIPs was moved to Soudan Mine in 2003.

3.4.2. ATHERMAL PHONONS AND IONIZATION CDMS II employs low-temperature ($<$50 mK) Ge (250 g) and Si (100 g) ZIP detectors (see Figure 9) that are operated at Soudan Mine, Minnesota (2070 mwe) (84). The detectors' fast superconducting transition edge sensors detect the nonthermal phonons from the particle interaction on time scales $\sim$1–100 μs.

For recoil energies above 10 keV, electron recoil events due to background photons are rejected with $>$99.9% efficiency, and surface events are rejected with $>$95% efficiency. Two different target materials are used so that the interaction rates and recoil spectrum shape of any candidate nuclear recoil signal in Ge and Si can be compared. For WIMPs interacting via spin-independent coupling, the expected coupling in Ge detectors is very much higher than that for Ge, whereas the interaction rate for neutrons is comparable.

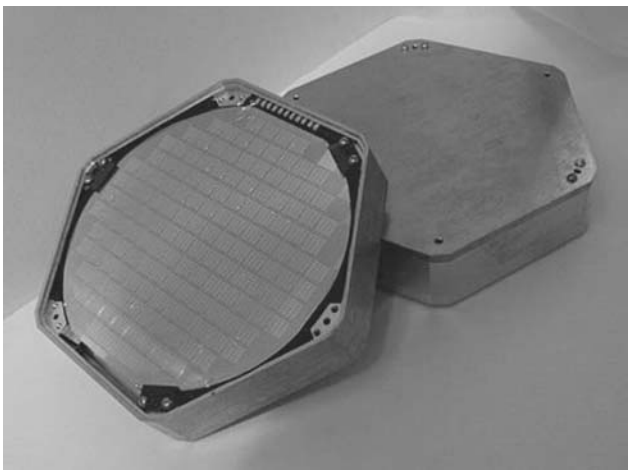

Figure 9 Mounted CDMS II ZIP detectors (75 mm diameter) made of either Ge (250 g) or Si (100 g).

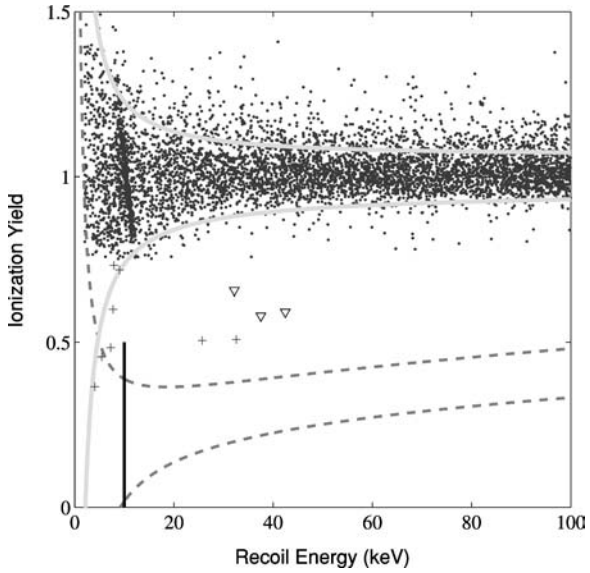

Figure 10 Ionization yield y versus recoil energy for WIMP-search data for four Ge detectors (total mass 0.75 kg) with a raw live time of 53 days from the CDMS II experiment (net exposure, after cuts, in 19.4 kg-days) (84). WIMP-search events for ionization yield, $y > 0.75$, are shown as points, $y < 0.75$ as geometrical shapes. The expected region for WIMP nuclear recoil events lies between the two lower dashed lines. The y value for the nuclear recoil events has a slight slope due to the energy dependence of the nuclear recoil quenching factor in Ge.

First results (84) from CDMS II show no nuclear recoil candidates from a run of 53 live days that, after cuts, yielded exposures of (Ge) 22 net kg–days and (Si) 5 net kg–days. Figure 10 shows a plot from the WIMP-search data; the ionization yield y (ionization energy/recoil energy) is shown versus recoil energy for events in the Ge detectors. The horizontal band at $y \sim 1$ occurs for electron recoil events. A few events, highlighted as geometrical shapes, show electron events that have incomplete charge collection due to surface effects. No WIMP-search events appear in the nuclear recoil band shown by dashed lines in Figure 10, which corresponds to a quenching factor of $\sim$30%. These results yield WIMP sensitivity limits that are a fourfold improvement over the latest results from Edelweiss. In situ energy calibrations were performed using external gamma and neutron sources. Close agreement of data and full detector/shield Monte Carlo simulations was obtained. Specifically, the shapes of the neutron recoil spectra were well matched in Ge and Si detectors, implying a 100% quenching factor for phonon channels for nuclear recoil versus gamma energy calibrations. The gamma calibrations create a specific category of events known as "ejectrons," which are characterized by electrons ejected from neighboring material (often an adjacent detector) onto the

ZIP detectors. These behave in a very similar fashion to surface beta contamination, allowing the calibration of the detectors to surface beta events.

3.4.3. PHONONS AND SCINTILLATION The CRESST Collaboration has been operating cryogenic detectors at Gran Sasso for more than five years. The thermal phonon detection uses a single-element (100 μm $\times$ 200 μm) superconducting phase transition (SPT) thermometer of alpha-phase W with $T_c \approx 7$–25 mK. The energy resolution of the SPT detectors is very good, with a typical 5σ trigger threshold of 1.8 keV_r in a 300 g Ca_2WO_4 target. Discrimination of electron and nuclear recoils is achieved by the simultaneous detection of the thermal phonons and a second signal, due to the scintillation of the Ca_2WO_4. The scintillation light is detected using an adjacent photon detector formed from a 30×30 mm Si wafer instrumented with a second SPT (133, 134). The effective threshold for detection of the light from electron recoils in the main target is 2.8 keV_{ee}. For O nuclear recoils in the main target crystal, it has been shown that the scintillation signal has a quenching factor of $\sim$14% relative to electron recoils. This leads to an effective threshold for scintillation light detection for a nuclear recoil of $\sim$20 keV_r. The collaboration is currently taking steps to reduce this threshold by improving light collection into the photon detector. Gamma calibrations to date show that electron recoil leakage into the nuclear recoil band is at a level of 2% for 10–20 keV_r, 0.3% for 15–25 keV_r, and 0.1% for >20 keV_r. At present, the quenching factor for scintillation light in Ca_2WO_4 for Ca and W nuclear recoils has not been established. Lindhard theory (135) would suggest that recoils of these more massive nuclei would be quenched by a greater degree than recoils for the lighter O nucleus. This would raise the effective threshold (in keV_r) for clear detection of the scintillation signal, and has direct ramifications, discussed below, for the unambiguous identification of WIMP signals.

3.5. Liquid Noble Elements

3.5.1. LIQUID Xe DETECTORS Three collaborations are currently developing liquid Xe (LXe)–based detectors for DM.

The ZEPLIN I experiment (136), which has a fiducial mass of 3 kg and a total mass of 6 kg, operated for 90 live days at Boulby Mine, UK (2800 mwe) in 2001–2002. This detector uses the scintillation pulse shape alone to make a relatively weak discrimination between nuclear recoil and electron recoil events. With 290 kg–days Xe of exposure, and an analysis threshold of 2 keV_{ee} (equivalent to 9 keV_r, given the measured quenching factor of 22% that is applicable for Xe when no electric field is applied), a limit comparable to that of Edelweiss (exposure 32 kg–days Ge) has been achieved. However, the background discrimination is becoming systematically limited, and this mode of discrimination is unlikely to be pursued further. The DAMA group also previously operated a LXe detector at Gran Sasso (137).

Future LXe-based search experiments will operate by detecting both the scintillation and ionization signals from interactions in the liquid. Interestingly, in this

case both the scintillation and ionization signals are quenched for nuclear recoils, but by different amounts, meaning that the ratio of these signals can still be used to discriminate electron and nuclear recoils. The scintillation signal is detected directly using PMTs (or other photodetectors). The ionization signal is detected by drifting the ionization signal in the LXe (using fields ∼0.2–5 kV/cm) and then extracted at the liquid surface (extraction field 7–10 kV/cm) into the gas phase. The extraction field also allows the electron in the gas to undergo electroluminescence (EL), in which secondary photons are emitted from the accelerated electrons. These photons are also detected as a secondary signal in photodetectors. The delay time between primary (short pulse, ∼40 ns) and secondary EL (∼1 μs) light gives the drift time of the electrons, which is directly related to the depth of the event (electron drift velocity in LXe is 2.2 mm/μs). The x-y position of the event can be determined by the centroid weighting of the secondary light signal. For operation with a drift field of ∼5 kV/cm, the estimated nuclear recoil quenching factor relative to electron recoils for the primary scintillation light is 50%, and that for the ionization signal is ∼1% (the precise value has yet to be determined).

The Japanese XMASS-DM (138, 139) Collaboration has operated a 1 kg LXe detector since 2003 in Kamioke Mine (2700 mwe), collecting both light and charge signals. The applied electron drift voltage used was in the low drift field regime of operation, specifically 0.25 kV/cm over a distance of 9 cm. This is sufficient to drift the majority of electrons arising from an electron recoil event, but it is insufficient to extract electrons from the initial excitation region arising from nuclear recoils (giving an effective quenching factor for the ionization signal of 0%). In such a dense ionization region, all the electrons recombine locally. This means that in this experiment a nuclear recoil event is identified by the presence of primary scintillation light, in the absence of a secondary signal from ionization electrons. As will be discussed in Section 4.2, this means that the background in a DM search can be elevated by anomalous events that, for whatever reason, yield signals in only one of the signal channels. This was indeed the case with the latest reported results; it is suggested that alpha particles in the Teflon liner of the detector lead to light/no-charge events. This effect is currently limiting the detector's sensitivity. A new LXe detector of 14 kg mass is currently nearing operatio underground.

The Boulby Collaboration intends to begin operation of the ZEPLIN II and III detectors underground in 2004 (140, 141). The ZEPLIN II detector uses 7 × 12.5 cm diameter PMTs, observing a 30 kg fiducial LXe target. The ZEPLIN III uses 31 × 5 cm diameter PMTs to observe a 6 kg LXe target with a 3.5 cm drift length. The pancake design (small drift length) used in the latter detector allows the application of drift voltage in the high field (>5 kV/cm) regime. This will maximize the efficiency of separating some of the ionization electrons from the primary interaction ionization cloud for nuclear recoil events before they recombine.

The XENON (142, 143) Collaboration, in the United States, is currently operating a 10 kg LXe detector above ground, which is the prototype for a XENON10 module that will be taken underground in 2005–2006. This detector is also designed

to allow operation in the high drift field regime. In addition, the novel introduction of a CsI photocathode directly in the LXe should further improve the measurement of the primary scintillation photons by converting them to electrons, which are then drifted out of the liquid as a tertiary ionization signal, with the inherent EL gain.

On a general note, in LXe under high drift field operation, electron recoils are expected to yield a detectable signal of ∼15 UV photons/keV_{ee} and ∼60 ionization electrons/keV_{ee}, and for nuclear recoils ∼8 UV photons/keV_r and ∼0.5–1 ionization electrons/keV_r. The last number still needs to be experimentally verified unambiguously. The efficiency for detecting the primary photon signal is a function of the solid angle coverage for the photodetectors, the reflectivity of the chamber walls, the transmission of photons through charge grids, total internal reflection at the LXe surface, and the quantum efficiency of the photodetectors (e.g., the photocathodes of PMTs have a typical quantum efficiency of ∼20% for UV photons). A considerable challenge in LXe detectors is to ensure that the detection thresholds are consistent with observing 10–20 keV_r DM recoil events in primary light. The EL gain phase in gas typically generates >300 photons per electron once extracted into the gas, so even individual electrons from the liquid can be detected by their EL light in the PMTs. The challenge with the secondary signal is to ensure that a few electrons do escape the initial recombination region of a nuclear recoil interaction site.

3.6. Gaseous Detectors

3.6.1. Gas TPCs The DRIFT collaboration (144, 145) has operated a 1 m^3 NID-TPC (negative ion drift time projection chamber) at Boulby Mine (2800 mwe) since 2002. The target material is gaseous CS_2, which at the operating pressure of 40 torr is a target mass of 167 g.

The main motivation for developing gaseous detectors relates to their ability to resolve the major axis of ionization tracks arising from nuclear recoil events. This information could be used to unambiguously verify the detection of WIMPs, and it permits the study of the velocity vector distribution of the local WIMP population in the Milky Way halo. At present, the gas detectors can only determine the axis of the recoil event, rather than the direction (i.e., no front-back discrimination, just front-side), since the variation in the ionization density along the tracks does not seem to show a measurable asymmetry. The collaboration estimates that ∼140 WIMP interactions (for events above expected analysis threshold ∼40 keV_r) will be required to establish 90% CL statistical evidence that the recoil event axis distribution is not isotropic, but rather consistent with standard halo models for the WIMP velocity distribution.

In addition, the gaseous detectors have very good discrimination between nuclear and electron recoil events. For nuclear and electron events of the same total gaseous ionization, the track lengths for the two types of events differ greatly. An event corresponding to a 19 keV_{ee} electron recoil or a 47 keV_r S recoil both

18 Aug 2004 18:39 AR AR228-NS54-10.tex AR228-NS54-10.sgm LaTeX2e(2002/01/18) P1: JRX

generate 1000 negative ion pairs in CS_2, but their track lengths are ∼40 mm and ∼4 mm, respectively. It is estimated that this should lead to background rejection in excess of 10^6.

The sensitivity of this experiment for searching for WIMPs that couple via spin-independent coupling is dominated by the S nuclei but is penalized because of the small size of this nucleus. The integrated recoil spectra (in events/kg/d) for Ge and S are compared in Figure 6. The sensitivity to 100 GeV WIMPs for a 167 g target of CS_2 is equivalent to 33 g of Ge. Thus, an exposure of >1000 days live would be required for the DRIFT-1 (1 m^3) module to reach the detection sensitivity of the latest CDMS II result, which was achieved with a live exposure of ∼50 days. Collecting sufficient statistics (∼140 events) to test the anisotropy of a WIMP signal once discovered will require a much larger detector. The new CDMS II cross-section limits would now require an array of 125×1 m^3 gas modules operated for two live years to yield a statistically significant asymmetry. However, this will be an important dynamical measurements of the WIMP velocity distribution once discovery has occurred. At present, this technology remains alone in being able to provide this information.

3.7. Axion Detectors

Axions can be detected by looking for $a \rightarrow \gamma$ conversion in a strong magnetic field (146). Such a conversion proceeds through the loop-induced $a\gamma\gamma$ coupling, whose strength $g_{a\gamma\gamma}$ is an important parameter of axion models. Currently two experiments searching for axionic DM are taking data. They both employ high-quality cavities. The cavity "Q factor" enhances the conversion rate on resonance, i.e. for $m_a c^2 = \hbar\omega_{\rm res}$, where $\omega_{\rm res}$ is the resonant frequency for photon emission in the cavity. Because the axion mass m_a, or equivalently f_a, is unknown, a search must be made of all resonant frequencies with a sensitivity that is sufficient to test theoretical predictions.

The Axion experiment based at LLNL began taking data in 1996 (147) and has excluded axions with mass 2.9–3.3 μeV as a major component of the dark halo of the galaxy, assuming that $g_{a\gamma\gamma}$ is near the upper end of the theoretically expected range (148). At present, the experiment uses conventional low-noise electronic amplifiers with a cavity operated at liquid ^{4}He temperatures. A planned electronics upgrade will implement low-noise SQUID (superconducting quantum interference device) amplifiers and cool the cavity further by using a dilution refrigerator. This will improve the sensitivity to allow exclusion of all theoretical models at the resonance frequencies scanned.

The CARRACK experiment is being operated in Kyoto, Japan (149). It uses an alternative sensing system based on Rydberg atoms excited to a very high state ($n \simeq 230$) to detect the microwave photons. This permits almost noise-free detection of single photons. Preliminary results exclude axions in a narrow range around 10 μeV for some plausible range of $g_{a\gamma\gamma}$. An upgrade of the experiment will be designed to probe a mass range of 2–50 μeV with a sensitivity covering all plausible axion models, if the axions form most of the DM.

18 Aug 2004 18:39 AR AR228-NS54-10.tex AR228-NS54-10.sgm LaTeX2e(2002/01/18) P1: JRX

4. BACKGROUNDS IN SEARCH EXPERIMENTS AND THEIR REDUCTION

Many of the background shielding issues related to DM direct detection, and other low-background underground experiments, have been addressed in another paper in this journal (150) but are also briefly summarized here.

4.1. Radioactive Backgrounds

The experiments require a significant reduction in gamma background. Unshielded, a rate of $\sim 10^4$ evts/keV/kg/d will be observed at low energies ($<30\ keV_{ee}$) in the region of interest for DM recoils, in a standard 1 kg Ge detector. The sources are primarily the ^{238}U and ^{232}Th decay chains, with photon energies up to 2.6 MeV, and from ^{40}K, which emits a 1.46 MeV photon. Conventional Pb shielding can be used to drive this down to $\sim$0.1–1 evts/keV/kg/d. The inner lining (a few cm) of the Pb will need to be low in ^{210}Pb to reduce the contribution from bremsstrahlung (from ^{210}Bi beta decay with 1.16 MeV endpoint) of the electrons. (A rate of 1 Bq/kg ^{210}Pb in an inner Pb shield will typically contribute $\sim$1 evt/keV/kg/d at low energies.) Reductions in gamma rate below this will be achieved through either an ultraclean passive shielding or some type of active gamma veto. Of course, many of the technologies in use for DM searches provide intrinsic gamma discrimination, and the effective contribution to the DM candidate signal is reduced by many orders of magnitude.

Considerable attention should be paid to sources of radioactivity close to the active volume of the detectors. Local beta and alpha contamination have both been shown to lead to events that can be misidentified as DM candidate events. Some specific examples of this were discussed in Section 3. In addition, Rn gas must be excluded from the region inside the Pb shield, typically using a hermetic enclosure and pure N_2 gas purge.

Neutrons can give rise to signals that are indistinguishable from those of DM interactions, given that both lead to nuclear recoils, and the energy spectra can be very similar. Thermal neutrons are not directly a problem because kinematically they are unable to deposit sufficient energy directly in the detectors; however, their capture on materials can lead to an additional gamma signal. Neutrons $\gtrsim$50 keV are able to generate recoils that are in the kinematic region of interest. Neutrons that arise from (α, n) reactions in the rock can be moderated using low-Z material shields (typically polyethylene, or paraffin, where 10 cm will reduce the above-threshold neutron flux by about an order of magnitude). Some attention should also be paid to neutrons generated within the shield by the same process, although given that most of the materials within the shield have been selected for low radioactivity, the expected event rate arising from this process are many orders of magnitude below current WIMP sensitivity limits.

A rogue neutron signal can, of course, be tagged in many of the detectors because the neutron scattering length is short enough that some fraction of events will appear as multiple scatters.

Muons directly interacting with the shielding material will generate neutrons. These events can be tagged directly by surrounding the shield with a muon veto. Vetos with efficiencies of >99% can be constructed, so this background should not limit an experiment.

High-energy neutrons are generated by cosmic ray muons in the surrounding cavern rock. Conventional moderator shielding has little effect on neutrons >20 MeV, and in general the contribution of neutrons with energies of 20–1000 MeV arising from muons must be considered. Monte Carlo simulations performed by the CDMS II experiment indicate that at a depth of 2070 mwe, the experiment will ultimately begin to be limited by high-energy "punch-through" neutrons at a rate of ∼0.003 /kg/d in the energy range 15–45 keV_r with a recoil spectrum that is similar to that from DM.

The high-energy neutron flux can be reduced by conducting experiments at deeper locations. Table 4 shows a relative comparison of the muon and expected high-energy neutron fluxes at a number of underground laboratories. For the sites <2.5 kmwe the differential muon flux is typically flat up to an energy (250 GeV/1 kmwe) and then falls at higher energies. For sites deeper than 2.5, kmwe the muon spectral shape remains constant and only the flux varies (151).

4.2. Confusion Thresholds and Anomalous Events

The ability to distinguish event-by-event between electron and nuclear recoils in a given detector arises because different mechanisms for reading out the "energy" of the event have different quenching factors (see Section 2.2). In the absence of systematic tails in the detector response, the effective energy threshold at which it is possible to distinguish nuclear from electron recoils is then set by the signal-to-noise ratio available in the readout channels. Naively, one might expect that greater

TABLE 4

Site (multiple levels given in ft)	Relative muon flux	Relative neutron flux T > 10 MeV
WIPP (2130 ft) (1500 mwe)	× 65	× 45
Soudan (2070 mwe)	× 30	× 25
Kamioke	× 12	× 11
Boulby	× 4	× 4
Gran Sasso (3700 mwe)		
Frejus (4000 mwe)	× 1	× 1
Homestake (4860 ft)		
Mont Blanc	$\times 6^{-1}$	$\times 6^{-1}$
Sudbury	$\times 25^{-1}$	$\times 25^{-1}$
Homestake (8200 ft)	$\times 50^{-1}$	$\times 50^{-1}$

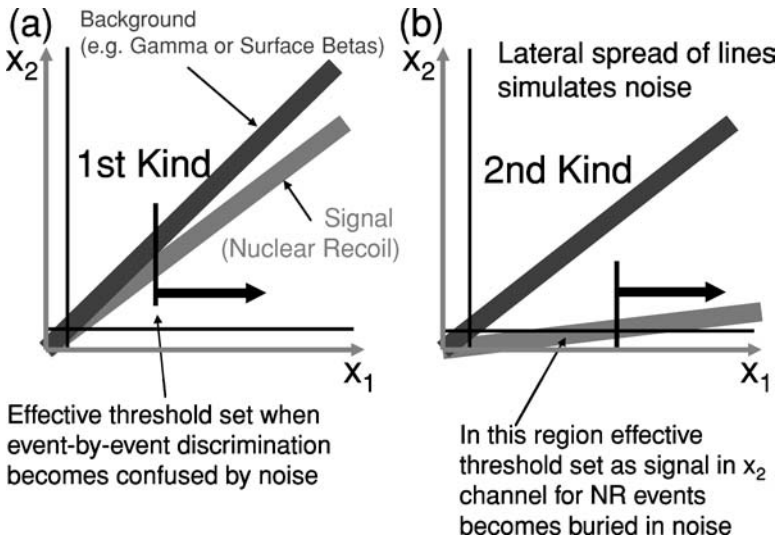

Figure 11 The plots represent background and signal event distributions in discriminating detectors, which use the ratio of measured quantities x_1 and x_2 to characterize the event. The two kinds of threshold effects arising from the relative ratios of the discrimination parameters are shown in (*a*), where signal and background distributions become confused, and (*b*), where x_2 falls into noise for signal events.

differences in the quenching factors will reduce the threshold for effective discrimination. However, because the DM recoil energy spectrum (in most scenarios) is a simple falling exponential, confusion can arise at low energies with simple noise events, with some other form of systematic, or with anomalous events. Establishing that the DM candidate signal has the correct behavior for nuclear recoils in two separate readout mechanisms will provide much stronger evidence for its presence than arguing that a candidate signal is present in one channel but is in the noise for the second.

Figure 11*a* shows a threshold effect of the "first kind," which arises because the intrinsic difference in the ratio of measured quantities x_2/x_1 for background and signal events is relatively modest. A region of confusion occurs for the event-by-event discrimination as the signal-to-noise ratio falls for low-energy events and the distributions start to overlap.

For example, in detectors based on phonon and ionization readout from cryogenic detectors, x_1 is the phonon signal (adjusted for the Luke Effect), and x_2 is the ionization signal. In Ge (Si) if x_2/x_1 for gamma events is 1, then x_2/x_1 for nuclear recoils is $\sim 1/3(1/2)$. The confusion threshold depends on the noise in the channels, and in the CDMS II experiment is below 5 keV_r for 10% overlap. The current Edelweiss experiment has greater noise in the charge readout and so has an overlap threshold which is ~ 10 keV_r.

Figure 11*b* shows a threshold effect of the "second kind." The ratio of the x_2/x_1 quenching factors is large. This would occur if nuclear recoil events produce far fewer excitations in the x_2 channel than do electron recoils of the same nominal recoil energy. The x_2 signal will probably fall into noise well before x_1. The CRESST experiment has been limited by this type of threshold effect, in which anomalous events with finite x_1 and no x_2 become confused with valid nuclear recoil events. One also has to consider the specific case of LXe detectors operated with low drift fields. In this case, no ionization signal can be extracted for nuclear recoil events, and x_2 is zero for all nuclear recoil events. The XMASS-DM experiment was operated in this mode. At low energies, the region of finite x_1 and no x_2 was populated by anomalous events, which reduced the overall sensitivity of the detectors.

In general, it is more difficult for backgrounds to provide the correct amount of signal in both x_1 and x_2 to fake nuclear recoil events. However, results from cryogenic ionization detector experiments have shown that electron recoil interactions very near the surface of the detectors do indeed have a reduced ionization yield that causes the events to leak into the nuclear recoil acceptance region. High-statistics calibrations of the detectors are required in order to establish the magnitude of this systematic tail in the response and so provide a limit on its likely contamination of the signal region.

5. PERSPECTIVES AND CONCLUSION

5.1. Resolving the Existing Annual Modulation Positive Signal

5.1.1. HALO MODELS If it is assumed that WIMPs interact with spin-independent coupling, it is not possible to reconcile the results of the DAMA experiment with the other direct detection results. Some questions have been raised concerning the possible influence of DM halo models when comparing results from different experiments, but the consensus appears to be that there is insufficient latitude in astrophysically reasonable halo models to explain the discrepancy.

It is true that the choice of halo model will affect the modulation signal and the overall rate differently. For example, a decrease in the higher-velocity tail will decrease the overall WIMP event rate above an appropriate threshold for detection. However, at the same time, the size of the modulation signal is increased because with fewer higher-velocity WIMPs the Earth's motion around the sun becomes a larger perturbation on the net WIMP velocity as measured in the detector frame of reference. In addition, adding a bias to the overall flow direction of the WIMPs (assumed isotropic within the galaxy in the isothermal model) relative to the direction of motion of the Earth will have a disproportionate effect on the annual modulation signal relative to the direct detection signal. Copi & Krauss (154) have directly addressed the issue of comparing annual modulation and direct detection, given the uncertainties due to galactic halo models. They present data summarizing how the DAMA annual modulation signal for a given halo model changes relative

to that for a standard halo. They compare the ratio of the change in the annual modulation amplitude to the ratio of the change for the direct detection signal for the new halo model relative to a standard halo. Their ratio of ratios would exceed 1 if the model brings about better agreement between the experiments. (That would imply that the appropriate cross section from the DAMA region would be lower than the cross section extracted using the standard halo, which would bring DAMA closer to the upper limits of the direct detection experiments.) An isothermal halo model with dispersion of 170 km/s would give the largest ratio of ratios, $\sim$2.8 for a 100 GeV WIMP. However, this adjustment is insufficient to reconcile the annual modulation amplitude with the direct detection experimental results. Green (156) has studied in some detail the effects of astrophysical uncertainties and some of the simplifying assumptions that are often made when calculating annual modulation signals. She concludes that approximations used for the Earth's motion around the sun and the sun's velocity with respect to galactic rest frame can introduce an error of up to 10 days in the phase and tens of percentage points in the shape of the signal, even when the WIMP velocity distribution is isotropic. She also considers how the annual modulation signal varies for physically and observationally well-motivated velocity distributions; she concludes that the phase may change by up to 20 days, and the mean value and amplitude change by up to tens of percentage points. The analysis focused on the logarithmic ellipsoidal halo models consistent with the constraints mentioned above. In addition, Green argues that a multivariate Gaussian velocity distribution, with axes corresponding to the axes of the halo and velocity dispersions with large ratios, is unlikely to correspond to a physically reasonable halo model. Clearly, her conservative analysis provides little succor in attempting to reconcile the current disagreement between annual modulation and direct detection. Copi & Kraus's conclusion, based on the direct detection data available in late 2002, is that halo model uncertainties do not allow a reconciliation of the DAMA result with the direct detection limits from Ge cryogenic detectors. The direct detection limits have since improved fivefold while the central value of the DAMA result remains unchanged (with an improved statistical significance from further running time).

Of course, in the event of a positive direct detection signal, comparison with annual modulation data could ultimately allow significant constraints on anisotropic halo models even before directional (axial) sensitivity data become available. Also, the deviations for annual sinusoidal behavior discussed by Fornengo & Scopel (157) may be used as a direct way of measuring, or setting limits, on the degree of anisotropy of the galactic halo. For the modulation signal, there are two important paramaters: the amplitude of the modulation as a fraction of the direct detection signal (or WIMP cross section) and the phase of the modulation. For symmetric halo models (such as the isothermal and Evans halos), since all directions through the halo are approximately equivalent, the modulation should be in phase with the motion of the Earth around the sun, representing an offset on the calendar year of 152.5 d. In triaxial models, Copi & Krauss show that this phase offset could shift to a phase offset of 35–65 d, with a specific dependency on the WIMP mass. This

should be compared with the best fit for modulation phase from DAMA of 144 ± 22 d (1σ) when a period of 1 y is assumed (124). It would seem that the DAMA data are already in disagreement with the triaxial models. Fornengo & Scopel (157) also concluded that strong radial anisotropies in the WIMP halo are excluded by the DAMA data. The main consequences of co-rotation and counter-rotation of the DM halo are as expected. In co-rotation, the decrease in the relative velocity between the WIMPs and the Earth leads to a smaller WIMP kinetic energy in the lab frame, and so heavier WIMPs are required to deposit the same characteristic recoil energy. The reverse is true for counter-rotation.

Belli et al. (158) have analyzed a broad range of galactic halo models in order to provide conservative limits on the spin-independent WIMP cross section that are consistent with the DAMA annual modulation signal. They consider spherical DM halos (with isotropic and nonisotropic velocity dispersion) axisymmetric and triaxial models that are consistent with astrophysical constraints. In addition, they model the consequences of co-rotation and counter-rotation. The combined data are presented in Figures 36 and 37 of their paper, which show the 3σ region of WIMP masses and WIMP cross sections. These results are consistent with the DAMA annual modulation amplitude if all astrophysically reasonable models are permitted. The cross section is quoted as $\xi\sigma_{\mathrm{scalar}}^{\mathrm{nucleon}}$, where ξ is the fractional amount of local nonbaryonic DM density that is ascribed to the WIMP responsible for the effect ($\xi \leq 1$). In the DAMA papers, this same symbol is used for the local density $\xi = \rho_\chi/(0.3\,\mathrm{GeV\,cm^{-3}})$, which leads to confusion when comparing results. When trying to compare the positive annual modulation signal results with the direct detection exclusion limits, one cannot simply take the allowed regions from the Belli paper. The data in this paper are provided for comparison with accelerator searches that are trying to establish the WIMP's properties by means independent of the halo properties. The direct detection results will also change when a different halo model is selected, and this must be taken into account. In particular, both annual modulation and direct detection limits will move by the same amount when ρ_χ changes relative to the usual normalization of $(0.3\,\mathrm{GeV\,cm^{-3}})$. It is clear that most of the changes in the relative positions of the loci of direct detection results from different experiments when using different halo models could be reduced by better choice of axes in WIMP mass–cross section plots. An appropriate choice would be $m_\chi\langle v^2\rangle/(220\,\mathrm{km/s})^2$ and $\sigma\rho_\chi/(0.3\,\mathrm{GeV\,cm^{-3}})$, where $\langle v^2\rangle$ suitably represents the local characteristic velocity of WIMPs at the detector for a model. Much of the remaining difference between the influence of a halo model on the ratio of annual modulation and direct detection results could be summarized by the variation of characteristic modulation amplitude over total direct interaction rate, much as Copi & Krauss presented.

5.1.2. WIMP NUCLEON COUPLING ALTERNATIVES As an alternative to resolve the current contradiction between DAMA and other direct detection results, a mechanism is required to suppress the detection rate in Ge/Xe versus NaI targets. Spin-dependent WIMP-nucleon couplings should be considered, since both the target

nuclei in NaI are mono-isotopic with an odd number of protons, whereas Ge and Xe detectors possess only a limited proportion of odd neutron isotopes. Considerable fine tuning is necessary in order to find a WIMP that will couple with such a great preference to odd proton spin alone (159). New direct detection technologies are being developed that will have significantly enhanced sensitivities to spin-dependent WIMPs (using F-based targets), such as the underground Bubble Chamber experiments planned by the Collar/Chicago group. Also, tighter constraints have recently been published on indirect detection rates from the sun (77).

It has been suggested that the signal could arise from the inelastic scattering of WIMPs that possess a complex split into two approximately degenerate scalars, or have a Dirac fermion splitting into two approximately degenerate Majorana fermions. With an appropriate tuning of the energy difference between the two states, this model can be used to explain why a signal was observed for ^{127}I recoils even though collisions with lighter Ge nuclei are heavily suppressed because of the difficulty of generating the necessary excitation of the WIMP in its rest frame. However, this model can be ruled out with the limits from a search experiment with a heavier nucleus (e.g., Xe), such as the limit provided by the ZEPLIN I experiment.

5.1.3. SYSTEMATIC CONTRIBUTIONS A possible weakness in the overall analysis of the DAMA annual modulation data stems from the failure to demonstrate that the event rate in the low energy bins would, in the absence of the proposed DM signal, be unmodulated. The WIMP detection argument rests solely on the observation of annual modulation of the total signal, with no direct method for distinguishing between signals due to WIMPs and those from backgrounds. The collaboration has been unable to identify any potential source of background that is modulated with sufficient amplitude in the lowest energy bins and not in higher energy bins (in which they have looked for modulation and find none). Obviously, "beam off" data taking is not possible because the WIMPs are all-pervasive and not shieldable, but some type of systematic check of the data-taking chain still needs to be performed very frequently. Although DAMA has established that the energy calibration is very stable at particular calibration energies, one cannot automatically infer that the energy calibration for all energies is necessarily as stable. Given that the DAMA experiment looks for fluctuations in individual bins, the integrity of the results depends on assuming that the stability of the differential linearity of the data taking is good to $\ll 2\%$ in the 2–4 keV_{ee} energy range. A fluctuation of a few percent in the energy calibration of the bin edges would modulate the count rate within the bin. The stability of the observed event rate of the bins in the 2–6 keV_{ee} range could be checked frequently by adding a known background using Compton scattering from gamma sources. This data would need to be taken with sufficiently high statistics for each run. Furthermore, data taking would have to be sufficiently frequent that the stability of the acceptance of background events was $\ll 2\%$ over all cycles of data taking. This would demand $> 10^5$ calibration events per energy bin, taken many times over the year.

18 Aug 2004 18:39 AR AR228-NS54-10.tex AR228-NS54-10.sgm LaTeX2e(2002/01/18) P1: JRX

The collaboration has reported that some Compton gamma calibrations were performed, but they were not sufficiently frequent to place any useful limit on the long-term stability of the acceptance to low-energy background events. The upgrade of DAMA's acquisition electronics in 2000 did allow multiple scatter events to be recorded rather than simply rejected, as in earlier data taking cycles. Clearly, events that hit multiple detectors cannot be due to WIMPs and so would represent a useful cross-check. The collaboration has reported an upper limit on the amount of modulation seen for multiple scatter events in the lowest energy bins, but statistically, these relatively rare events fail to provide a sufficiently stringent limit on the stability of the event acceptance.

In order to make a claim for an effect at the 1% level, the required control of systematics means that the experiment needs to spend as much time calibrating as taking real data. A simple example of how differential nonlinearity can be introduced into an experiment is through the wandering of a baseline voltage at the input of an ADC. It is common for high-speed ADCs to show some differential nonlinearity, which will be differently sampled if the input baseline moves.

It is also of concern that to date the collaboration has been unable to demonstrate a full model (through Monte Carlo simulations of the backgrounds) for the observed shape of the background spectra, after cuts and adjusted for efficiencies. In particular, there are significant differences in the reported low-energy event rates seen in the individual detectors (see Figure 2 of Reference (125)). In any given detector, the 2–3 keV bin has an event rate typically less than half that of the next highest energy bin, although even this ratio shows considerable variation across the array of nine detectors. There has been no quantitative demonstration of a consistent model for the pattern of radioactive backgrounds in the 2–15 keV range. Because so much of the statistical evidence for annual modulation comes from the lowest energy bin, it would seem prudent to demonstrate a clear understanding of how the background and proposed WIMP signal should combine to reproduce the observed background in each of he detectors. The number of counts in each keV bin is huge over the entire seven-year run ($\sim 10^5$ counts), so the variations in spectrum shape between the detectors are not statistical. Under many of the WIMP models consistent with the annual modulation data, a significant fraction of the events in the lowest energy bin will be due to WIMPs, and so the actual background contribution to the event rate needs to drop even more precipitously than the raw numbers suggest. The difficulty in explaining the published energy spectra at low energies, which are adjusted for cuts and efficiencies, seems to call into question whether the cuts and efficiencies are being correctly estimated. The event rate of noise and background events before cuts in the 2–3 keV bin is reported (125) to be 10 evts/keV/kg/d, so the noise cuts are removing $>90\%$ of events before the post-cut numbers are adjusted for estimated efficiency for real events.

As a general point, it is critical for an experiment that is reporting results based on a very subtle variation in the number of counts in its lowest energy bins to establish a clear method for demonstrating that the observed effect is not due to a simple modulation in the acceptance of background events. The collaboration

has demonstrated that it can rule out all suggested mechanisms. However, this is a necessary but not sufficient criterion for confidence in the final result. It is still possible that an as-yet-unchecked source of instrumental modulation is producing a June–December variation of 1.7% in the lowest energy bins. The fact that an instrumental effect is annual and has a phase of June–December could be an unhappy coincidence. Long-term environmental changes in, say, cavern temperature (which could influence electronics stability), or in ground water levels (which modify low-energy neutron fluxes), are possible candidates for summer-winter modulation.

5.2. Have We Got What It Takes to Discover Dark Matter Directly?

Part of the recent need to consider the construction of larger DM detectors has arisen because more sophisticated SUSY-based calculations are being performed, which indicate that WIMP-nucleon cross sections could be significantly lower than current sensitivities. However, existing experiments are also testing predictions of some SUSY models (see Figure 4). The rate at which detection sensitivities have been improving in the past five years is very encouraging. The challenge of constructing better DM detectors is being met by many separate groups—a (nearly) exhaustive list of whom is provided in Tables 3 and 4.

Experimentalists are often urged to ignore the predictions of theorists and to hunt for new particles regardless, by any means that are at hand. Precedent indicates that it may be prudent not to put too much weight on particular theoretical machinations; however, it is an important feature of WIMPs that they are motivated by both particle physics and cosmology. Unfortunately, within SUSY the link between the WIMP annihilation cross section and the WIMP-quark cross section is fairly loose. Whereas the former is determined rather precisely by cosmological bounds (Ω_m), the latter ranges over many orders of magnitude.

If we see SUSY at accelerators within this decade, then it is hoped that enough parameters will be determined to allow calculation of the LSP properties to determine if it can be CDM and, if so, what the LSP quark interaction rate will be.

Obviously, the DM community hopes to discover non-standard-model physics before this! It remains a tantalizing possibility that a number of the current experiments may observe an unequivocal signature for SUSY WIMPs (corresponding to an interaction rate that is at the upper end of the theoretically allowed range), and thereby provide a single answer to two of the more fundamental riddles in particle physics and cosmology.

ACKNOWLEDGMENTS

I thank my students Michael Attisha and John-Paul Thompson for their assistance in preparing this review. In addition, I thank many of my colleagues for their

comments and insights in this rapidly moving field. I know that they share my excitement about the results that are likely to unfold in this decade. We were sorry to learn in 2003 of the death of Angel Morales (Zaragosa), a leader in the field of experimental dark-matter-search physics. He will be sadly missed.

The *Annual Review of Nuclear and Particle Science* is online at http://nucl.annualreviews.org

LITERATURE CITED

1. Rumsfeld D. Department of Defense news briefing, Feb. 12 (2002)
2. Zwicky F. *Helv. Phys. Acta* 6:110 (1933)
3. Persic M, Salucci P, Stel F. *Mon. Not. R. Astron. Soc.* 281:27 (1996)
4. Battaner E, Florido E. *Fund. Cosmic Phys.* 21:1 (2000)
5. Binney J, Tremaine S. *Galactic Dynamics.* Princeton, NJ: Princeton Univ. Press (1988)
6. EROS Collab. *Astron. Astrophys.* 400:951 (2003)
7. Alcock C, et al. (MACHO Collab.) *Ap. J.* 542:281 (2000)
8. Freedman WL. *Phys. Scripta* T85:37 (2000)
9. Peebles J. *Ap. J.* 263:L1 (1982)
10. Primack JR. *Proc. Midrasha Mathematicae in Jerusalem: Winter School in Dynamical Systems, Jerusalem, Israel* (1997), astro-ph/9707285
11. Hinshaw G, et al. *Ap. J.* 464:L17 (1996)
12. de Bernardis P, et al. *Nature* 404:955 (2000)
13. Lee AT, et al. *Ap. J.* 561:L1 (2001)
14. Padin S, et al. *Ap. J.* 549:L1 (2001)
15. Kovac J, et al. *Nature* 420:772 (2002)
16. Bennet CL, et al. *Ap. J. Suppl.* 148:1 (2003)
17. Prada F, et al. *Astrophys. J.* 598:260 (2003)
18. Schramm DN, Turner MS. *Rev. Mod. Phys.* 70:303 (1998)
19. Cyburt RH, Fields BD, Olive KA. *Phys. Lett.* B567:227 (2003)
20. Tytler D, et al. *Ap. J.* In press (2004), astro-ph/0403688
21. Barris BJ, et al. *Ap. J.* 602:571 (2004)
22. Knop RA, et al. (Supernova Cosmology Project). *Ap. J.* 598:102 (2003)
23. Tonry JL, et al. *Ap. J.* 594:1 (2003)
24. Spergel DN, et al. *Ap. J. Suppl.* 148:175 (2003)
25. Tegmark M, et al. *Phys. Rev. D* 69:103501 (2004)
26. Fukuda Y, et al. *Phys. Rev. Lett.* 81:1562 (1998)
27. Ahmad QR, et al. (SNO Collab.) *Phys. Rev. Lett.* 89:011301 (2002)
28. Kolb EW, Turner ME. *The Early Universe.* Cambridge, MA: Perseus (1994)
29. Jungman G, Kamionkowski M, Griest K. *Phys. Rep.* 267:195 (1996)
30. Dress J (LEP Collab., LEP Electroweak Work. Group). Presented at Int. Symp. Lepton and Photon Interactions at High Energy, XXth, Rome, Italy (July 2001)
31. Peccei RD, Quinn HR. *Phys. Rev. Lett.* 38:1440 (1977)
32. Eidelman S, et al. *Phys. Lett.* B592:216 (2004)
33. Rajagopal K, Turner MS, Wilczek F. *Nucl. Phys. B* 358:447 (1991)
34. Covi L, Roszkowski L, Small M. *J. High Energy Phys.* 0207:023 (2002)
35. Covi L, Roszkowski L, Ruiz de Austri R, Small M. hep-ph/0402240
36. Chung DJH, Kolb EW, Riotto A. *Phys. Rev. D* 59:023501 (1999)
37. Chung DJH, Kolb EW, Riotto A. *Phys. Rev. Lett.* 81:4048 (1988)
38. Carr BJ, Hawking SW. *MNRAS* 168:399 (1974)

39. Cheng HC, Feng JL, Matchev KT. *Phys. Rev. Lett.* 89:211301 (2002)
40. Primack JR, Seckel D, Sadoulet B. *Annu. Rev. Nucl. Part. Sci.* 38:751 (1988)
41. Smith PF, Lewin JD. *Phys. Rep.* 187:203 (1990)
42. Bergstrom L. *Rep. Prog. Phys.* 63:793 (2000)
43. Gondolo P. Presented at NATO Advanced Study Inst. "Frontiers of the Universe" (Sept. 2003), astro-ph/0403064
44. Munoz C. *Int. J. Mod. Phys. A* In press (2004), hep-ph/0309346
45. Eidelman S, et al. *Phys. Lett.* B592:216 (2004)
46. Goldberg H. *Phys. Rev. Lett.* 50:1419 (1983)
47. Ellis JR, et al. *Nucl. Phys. B* 238:453 (1984)
48. Arnowitt R, Dutta B, Hu B. *Beyond The Desert '03*, Castle Ringberg, Germany (June 2003), hep-ph/0310103
49. Ellis JR, Olive KA, Santoso Y, Spanos VC. *Phys. Lett.* B565:176 (2003)
50. Alam MS, et al. (CLEO Collab.) *Phys. Rev. Lett.* 74:2885 (1995)
51. Ellis JR, Falk T, Olive KA, Santoso Y. *Nucl. Phys. B* 652:259 (2003)
52. Du DS, et al. *Phys. Rev. D* 65:094025 (2002); erratum, 66:079904 (2002)
53. Beneke M, Buchalla G, Neubert M, Sachrajda CT. *Phys. Rev. Lett.* 83:914 (1999)
54. ALEPH Collab., et al. hep-ex/0107030
55. Baer H, Balazs C, Belyaev A, O'Farrill J. *JCAP* 0309:007 (2003)
56. Chattopadhyay U, Corsetti A, Nath P. *IVth Int. Conf. Non-Accelerator New Physics (NANP'03)*, Dubna, Russia (June 2003), hep-ph/0310228
57. Bennett GW, et al. *Phys. Rev. Lett.* 92: 161802 (2004)
58. Roszkowski L. *Pramana* 62:1 (2004), hep-ph/0404052
59. Goto T, Nihei T. *Phys. Rev. D* 59:115009 (1999)
60. Babu KS, Pati JC, Wilczek F. *Nucl. Phys. B* 566:33 (2000)
61. Murayama H, Pierce A. *Phys. Rev. D* 65:055009 (2002)
62. Bertone G, Hooper D, Silk J. hep-ph/0404174
63. Bottino A, Donato F, Fornengo N, Scopel S. *Phys. Rev. D* 69:037302 (2004)
64. Lahanas AB, Nanopoulos DV. *Phys. Lett.* B568:55 (2003)
65. Baltz EA, Gondolo P. *Phys. Rev. D* 67: 063503 (2003)
66. Ellis J, et al. *Eur. Phys. J. C* 24:311 (2002)
67. Battaglia M, et al. *Eur. Phys. J. C* 33:273 (2004)
68. Bernabei R, et al. *Phys. Lett.* B480:23 (2000)
69. Gaitskell RJ, Mandic V. *Dark matter direct detection results plotter.* (2004) http://dmtools.brown.edu, http://dmtools.berkeley.edu
70. Kamionkowski M, Griest K, Jungman G, Sadoulet B. *Phys. Rev. Lett.* 74:5174 (1995)
71. Bergstrom L, Ullio P, Buckley JH. *Astropart. Phys.* 9:137 (1998)
72. Gondolo P, Silk J. *Phys. Rev. Lett.* 83:1719 (1999)
73. Ullio P, Kamionkowski M, Vogel P. *J. High Energy Phys.* 0107:044 (2001)
74. Ahrens J, et al. (AMANDA Collab.) *Phys. Rev. D* 66:032006 (2002)
75. Baltz EA, Edjso J, Freese K, Gondolo P. *Phys. Rev. D* 65:063511 (2002)
76. Duda G, et al. *Phys. Rev. D* 67:023505 (2003)
77. Desai S, et al. (Super-Kamiokande Collab.) *Phys. Rev. D* In press (2004) hep-ex/0404025
78. Smith D, Weiner N. *Phys. Rev. D* 64: 043502 (2001)
79. Goodman MW, Witten E. *Phys. Rev. D* 31:3059 (1985)
80. Helm RH. *Phys. Rev.* 104:1466 (1956)
81. Lewin JD, Smith PF. *Astropart. Phys.* 6:87 (1996)
82. Ressel RT, Dean DJ. *Phys. Rev. C* 56: 535

83. Tovey DR, et al. *Phys. Lett.* B488:17 (2000)
84. Akerib D, et al. (CDMS Collab.) *Phys. Rev. Lett.* In press (2004), astro-ph/0405033
85. Gaitskell RJ, et al. *Nucl. Phys. B (Proc Suppl.)* 51:279 (1996)
86. Drukier AK, Freese K, Spergel DN. *Phys. Rev. D* 33:3495 (1986)
87. Freese K, Friedman J, Gould A. *Phys. Rev. D* 37:3388 (1988)
88. Spergel D. *Phys. Rev. D* 37:1353 (1988)
89. Hasenbalg F. *Astropart. Phys.* 9:339 (1998)
90. Vergados JD. *Phys. Rev. D* 67:103003 (2003)
91. Copi CJ, Heo J, Krauss LM. *Phys. Lett.* B461:43 (1999)
92. Morales A. *Nucl. Phys. B (Proc. Suppl.)* 114:39 (2003)
93. Mosca L. *Nucl. Phys. B (Proc. Suppl.)* 114:59 (2003)
94. Arnaboldi C, et al. (CUORE Collab.) *Astropart. Phys.* 20:91 (2003)
95. Abplanalp M, et al. *Nucl. Instrum. Methods A* 370:227 (1996)
96. Cebrian S, et al. *Astropart. Phys.* 15:79 (2001)
97. Cebrian S. et al. *Phys. Lett.* B563:48 (2003)
98. Miuchi K, et al. *Astropart. Phys.* 19:135 (2003)
99. Bradley DI, et al. *Phys. Rev. Lett.* 75:1887 (1995)
100. Ahlen SP, et al. *Phys. Lett.* B195:603 (1987)
101. Reusser D, et al. *Phys. Lett.* B255:143 (1991)
102. Beck M, et al. (Heidelberg-Moscow Collab.) *Phys. Lett.* B336:141 (1994)
103. Garcia E, et al. *Phys. Rev. D* 51:1458 (1995)
104. Baudis L, et al. *Phys. Rev. D* 63:022001 (2001)
105. Morales A, et al. *Phys. Lett.* B532:8 (2002)
106. Caldwell DO, et al. *Phys. Rev. Lett.* 65:1305 (1990)
107. Gaitskell RJ, et al. Majorana Collab. White Paper nucl-ex/0311013
108. Klapdor-Kleingrothaus HV. *Nucl. Phys. B* 110:364 (2002)
109. Bacci C, et al. *Phys. Lett.* B293:460 (1992)
110. Bottino A, et al. *Phys. Lett.* B295:330 (1992)
111. Bernabei R, et al. *Phys. Lett.* B389:757 (1996)
112. Bernabei R, et al. *Phys. Lett.* B389:757 (1996)
113. Fushimi K, et al. *Phys. Rev. C* 47:R425 (1993)
114. Fushimi K, et al. *Nucl. Phys. B (Proc. Suppl.)* 35:400 (1994)
115. Quenby J, et al. *Phys. Lett.* B351:70 (1995)
116. Smith PF, et al. *Phys. Lett.* B379:299 (1996)
117. Smith PF, et al. *Phys. Rep.* 307:275 (1998)
118. Gerbier G, et al. *Astropart. Phys.* 11:287 (1999)
119. Ahmed B, et al. *Astropart. Phys.* 19:691 (2003)
120. Kudryavtsev VA, et al. *Astropart. Phys.* 17:401 (2002)
121. Sarsa ML, et al. *Phys. Lett.* B386:458 (1996)
122. Sarsa ML, et al. *Phys. Rev. D* 56:1856 (1997)
123. Bernabei R, et al. *Phys. Lett.* B424 (1998)
124. Bernabei R, et al. *Riv. Nuovo Cim.* 26:1 (2003)
125. Bernabei R, et al. *Eur. Phys. J. C* 18:283 (2000)
126. Cebrian S, et al. *Nucl. Phys. B (Proc. Suppl.)* 114:111 (2003)
127. Gerbier G, et al. (Edelweiss Collab.) Presented at TAUP Conf., 8th, Univ. Washington, Seattle, WA, Sep. 5–9 (2003)
128. Benoit A, et al. (Edelweiss Collab.) *Phys. Lett.* B545:43 (2002)
129. Luke PN. *J. Appl. Phys.* 64:6858 (1988)
130. Abusaidi R, et al. *Phys. Rev. Lett.* 84:5699 (2000)

131. Akerib D, et al. (CDMS Collab.) *Phys. Rev. D* 68:082002 (2003)
132. Shutt T, et al. *Nucl. Instrum. Methods A* 444:340 (2000)
133. Bravin M, et al. *Astropart. Phys.* 12:107 (1999)
134. Meunier P, et al. *Appl. Phys. Lett.* 75:1335 (1999)
135. Lindhard J, et al. *Mat. Fys. Medd. Dan. Vid. Selsk.* 10:1 (1963)
136. Smith NJT, et al. *Proc. 4th Int. Workshop Identification of Dark Matter*, p. 302. Singapore: World Sci. (2003)
137. Bernabei R, et al. *Phys. Lett.* B436:379 (1998)
138. Suzuki Y, et al. *Proc. 3rd Int. Workshop Low Energy and Solar Neutrinos, Sudbury, Canada, June 15 (2000)*, hep-ph/0008296
139. Yamashita M, et al. *Astropart. Phys.* 20:79 (2003)
140. Kudryavtsev VA. (Boulby Dark Matter Collab.) *Nucl. Phys. B (Proc. Suppl.)* 118:526 (2003)
141. Araujo HM, et al. *Nucl. Instrum. Methods A* 521:407 (2004)
142. Aprile E, et al. *Proc. Int. Workshop Techniques and Applications of Xenon Detectors (Xenon01), ICRR, Univ. of Tokyo, Kashiwa, Japan.* Singapore: World Sci. (2002)
143. Yamashita M, et al. *Nucl. Instr. Methods A* In press (2004)
144. Snowden-Ifft DP, Martoff CJ, Burwell JM. *Phys. Rev. D* 61:101301 (2000)
145. Ohnuki T, Snowden-Ifft DP, Martoff CJ. *Nucl. Instrum. Methods A* 463:142 (2001)
146. Sikivie P. *Phys. Rev. Lett.* 51:1415 (1983); erratum, 52:695 (1984)
147. Peng H, et al. *Nucl. Instrum. Methods A* 444:569 (2000)
148. Asztalos S, et al. *Phys. Rev. D* 64:092003 (2001)
149. Tada M, et al. physics/0101028
150. Formaggio J, Martoff J. *Annu. Rev. Nucl. Part. Sci.* 54:In press (2004)
151. Groom DE, et al. *Eur. Phys. J. C* 15:1 (2000)
152. Kamionkowski M, Kinkhabwala A. *Phys. Rev. D* 57:3256 (1998)
153. Ullio P, Kamionkowski M. *J. High Energy Phys.* 0103:049 (2001)
154. Copi CJ, Krauss LM. *Phys. Rev. D* 67: 103507 (2003)
155. Copi CJ, Krauss LM. *Phys. Rev. D* 63: 043507 (2001)
156. Green AM. *Phys. Rev. D* 68:023004 (2004)
157. Fornengo N, Scopel S. *Phys. Lett.* B576: 189 (2003)
158. Belli P, Cerulli R, Fornengo N, Scopel S. *Phys. Rev. D* 66:043503 (2002)
159. Kurylov A, Kamionkowski M. *Phys. Rev. D* 69:063503 (2004)

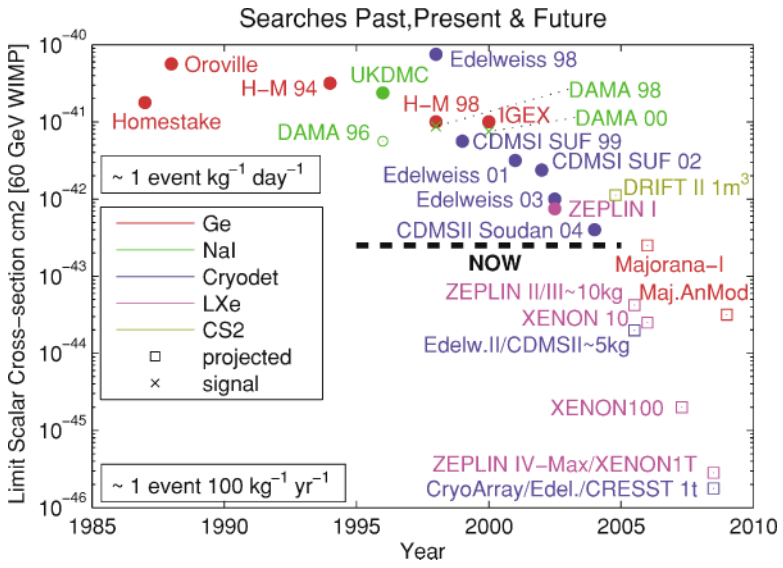

Figure 1 A selection of experiments' 90% upper CL results for 60 GeV WIMP-nucleon scalar cross section versus times of publications. Labels in boxes give the equivalent event rates in Ge in events/kg/day assuming a low recoil threshold, >10 keV.

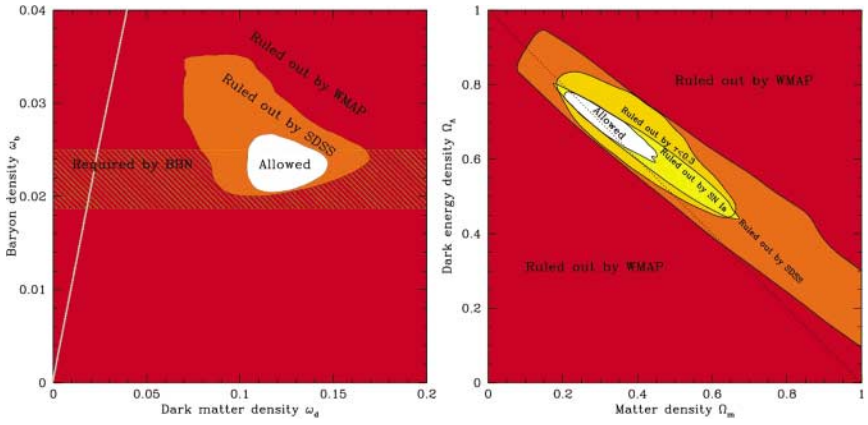

Figure 2 Observational constraints when combining data from WMAP, SDSS, SNIa, and BBN measurements, plus reionization optical depth limitation ($\tau < 0.3$) showing the 95% CL contours in the ($\omega_d = [\Omega_m - \Omega_b]h^2$, $\omega_m = \Omega_m h^2$) and (Ω_m, Ω_Λ) planes as constraints are added. The allowed region where the observations are consistent is shown unshaded. The grey diagonal line in the (ω_d, ω_m) plane indicates models with no additional DM component. The dotted diagonal line in the (Ω_m, Ω_Λ) plane indicates flat geometry for the universe, with open (closed) models below (above) this line (25).

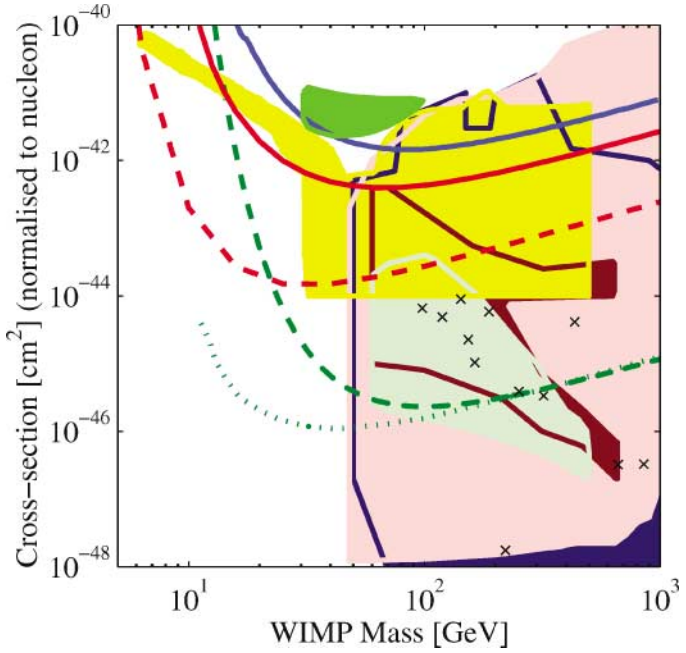

Figure 4 Theoretical models and experimental results for spin-independent WIMP-nucleon cross section versus WIMP mass. The theory regions are shown in yellow (Reference (63); artificial truncation of region at right and bottom edges), light green (64), dark red (55), dark blue (65), and light red (??), and the black crosses are benchmarks from References (66) and (67). Experimental data are shown from highest to lowest for reference, showing the DAMA allowed region in green (68), Edelweiss in blue (127), CDMS II in red (84), and projected sensitivities for (dashed red) CDMS II, (dashed green) XENON1T, and (dotted green) ZEPLIN IV-Max. The lowest experimental projection (dotted curve) represents an event rate of ~20 evts/tonne/y. Further data can be obtained from the DM direct detection results plotter (69).

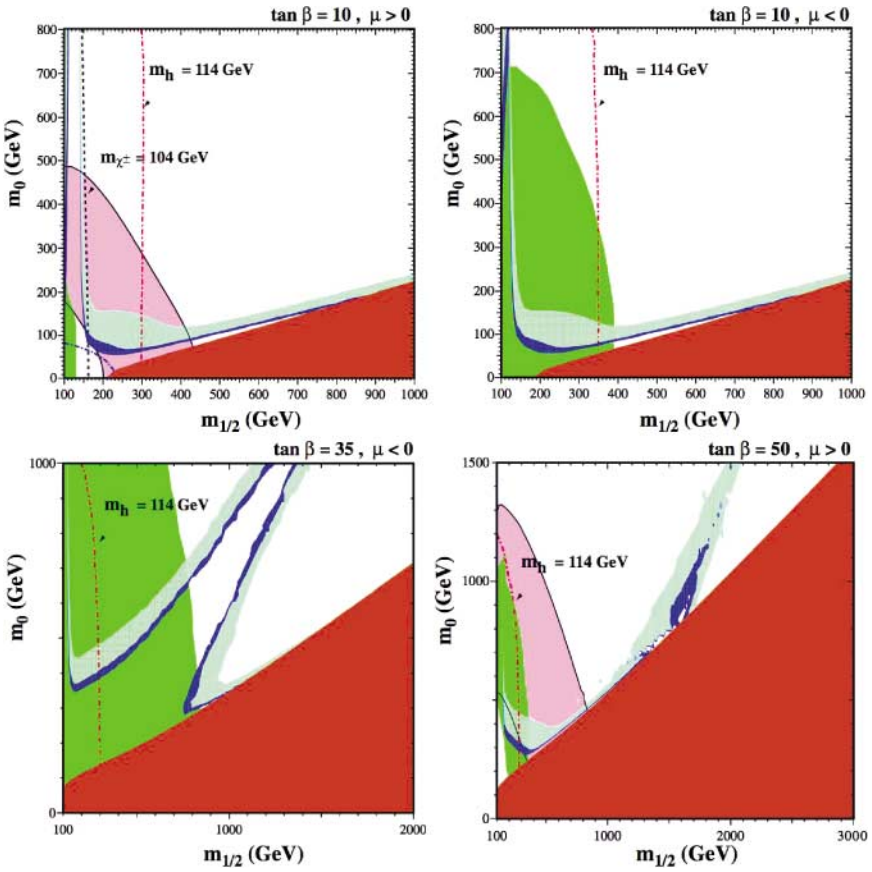

Figure 5 The ($m_{1/2}$, m_0) planes for a number of SUSY models taken from Ellis et al. (49). The panels are referenced (*a*)–(*d*), top left to bottom right. (*a*) tan β = 10, μ > 0, (*b*) tan β = 10, μ < 0, (*c*) tan β = 35, μ < 0, (*d*) tan β = 50, μ > 0. In each panel, the narrow, geometrically hyperbolic-like regions show the allowed regions based on older (light blue) and newer (dark blue) cosmological constraints, which are $0.1 \leq \Omega_\chi h^2\, h^2 \leq 0.3$, and $0.094 \leq \Omega_\chi h^2\, h^2 \leq 0.129$ (WMAP), respectively. The disallowed region occupying the lower-right quadrant (brown) comes from stop mass constraints ($m_{\tau 1} < m_\chi$). The disallowed region along the left edge (green) comes from $b \rightarrow s\gamma$. Panels *a* and *d* show models that are favored by $g_\mu - 2$ at the 2σ level, which is indicated by the pink shading in the lower left quadrant. The near-vertical dashed lines relate to contours based on the particle masses as indicated by the arrows.

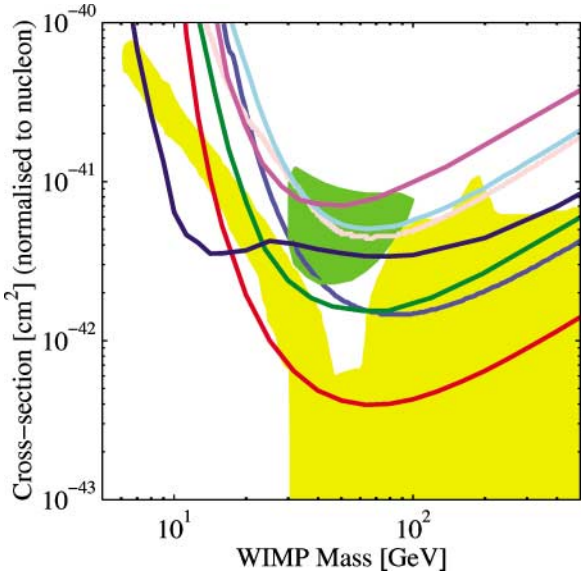

Figure 7 Recent experimental results for spin-independent WIMP-nucleon cross section versus WIMP mass. The DAMA allowed region is shown in green (68). The 90% CL exclusion limits from the experimental data are, from highest to lowest on the right-hand edge, those of IGEX (magenta) (105), DAMA (pulse-shape exclusion; cyan) (112), CRESST (2004 preliminary result; light red), CDMS(SUF) (dark blue) (131), ZEPLIN (2002 preliminary result; dark green) (136), Edelweiss (blue) (127), and CDMS II (red) (84). The lowest experimental curve represents an interaction rate of ~1 evt/kg/week. The yellow shaded region represent theoretical predictions from Bottino et al. (63). All curves assume standard DM halo parameters. Further data can be obtained from the DM direct detection results plotter (69).